NSWC TR 82-488

AD A132088

SHOCKWAVES IN FRESH WATER GENERATED BY THE DETONATION OF PENTOLITE SPHERES

BY T. P. LIDDIARD,
J. W. FORBES

RESEARCH AND TECHNOLOGY DEPARTMENT

28 MAY 1983

Approved for public release, distribution unlimited.

NAVAL SURFACE WEAPONS CENTER

Dahlgren, Virginia 22448 • Silver Spring, Maryland 20910

UNCLASSIFIED

SECURITY CLASSIFICATION OF THIS PAGE (When Data Entered)

REPORT DOCUMENTATION PAGE		READ INSTRUCTIONS BEFORE COMPLETING FORM
1. REPORT NUMBER NSWC TR 82-488	2. GOVT ACCESSION NO.	3. RECIPIENT'S CATALOG NUMBER
4. TITLE (and Subtitle) SHOCKWAVES IN FRESH WATER GENERATED BY THE DETONATION OF PENTOLITE SPHERES		5. TYPE OF REPORT & PERIOD COVERED Technical Report Oct 1979-Oct 1982 6. PERFORMING ORG. REPORT NUMBER
7. AUTHOR(s) T. P. Liddiard and J. W. Forbes		8. CONTRACT OR GRANT NUMBER(s)
9. PERFORMING ORGANIZATION NAME AND ADDRESS NAVAL SURFACE WEAPONS CENTER (Code R13) White Oak, Silver Spring, Maryland 20910		10. PROGRAM ELEMENT, PROJECT, TASK AREA & WORK UNIT NUMBERS 62633N Subproject #SE33-337-691
11. CONTROLLING OFFICE NAME AND ADDRESS Naval Sea Systems Command Washington, D. C. 20362		12. REPORT DATE 26 May 1983 13. NUMBER OF PAGES 59
14. MONITORING AGENCY NAME & ADDRESS(if different from Controlling Office)		15. SECURITY CLASS. (of this report) UNCLASSIFIED 15a. DECLASSIFICATION/DOWNGRADING SCHEDULE

16. DISTRIBUTION STATEMENT (of this Report)

Approved for public release, distribution unlimited.

17. DISTRIBUTION STATEMENT (of the abstract entered in Block 20, if different from Report)

18. SUPPLEMENTARY NOTES

19. KEY WORDS (Continue on reverse side if necessary and identify by block number)

Underwater
Shockwaves
Explosives
Pressure Measurements
High Speed Photography

20. ABSTRACT (Continue on reverse side if necessary and identify by block number)

Shock velocities as a function of distance were determined by differentiating distance-time paths of the shock waves. The distance-time information was obtained from high-speed photographs of the shocks obtained by a shadowgraphing technique. In addition, peak pressure and pulse time histories were recorded using lithium niobate gages. Pentolite spheres of three different initial radius (R_0) were used in the gage experiments. The shock velocities were obtained for relative distances of R/R_0 ranging from 1.2 to 4.0 while

DD FORM 1473 EDITION OF 1 NOV 65 IS OBSOLETE

UNCLASSIFIED

SECURITY CLASSIFICATION OF THIS PAGE (When Data Entered)

the pressure data were obtained for R/R_0 ranging from 4.4 to 12.3. Scalability of peak pressure and pulse half-widths times as a function of R/R_0 was successfully demonstrated. An analytical form was found that fits the peak pressure data from R/R_0 of 1 to 12.

FOREWORD

This work was performed for and funded by the NAVSEA Explosives Development, Effects and Safety block program, SF33-337-691. The results and conclusions presented in this report concerning shock waves in water from detonating pentolite spheres should be of interest to those seeking underwater sensitivity information and/or underwater damage information.

The authors wish to acknowledge the assistance of J. Marshall and A. Brown in conducting the lithium niobate gage experiments; D. Gillmore and R. Baker for conducting the underwater sensitivity experiments from which the shock velocities in water were obtained. H. Jones and J. W. Forbes obtained the gage information on the 6.84 cm radius pentolite sphere. Keith Harrison provided electronics support and ran many of the computer programs used for data reduction.

Approved by:

J. F. PROCTOR, Head
Energetic Materials Division

CONTENTS

ILLUSTRATIONS

TABLES

INTRODUCTION

The generation of spherical shock waves in water is of considerable interest to researchers and theoreticians. Spherical shock-generating systems in water have been used to study the behavior of shock waves, the effect of the shock waves against submerged structures, and interactions of the shock waves with other spherical shock waves.[1] These shock-generating systems also have been used to induce detonation in explosive samples placed at various distances from a spherical donor.[2,3] Such a system was used by Liddiard[4] to detect chemical reaction in test samples at pressures as low as 4 kbar in the sample or 3 kbar in water.

In applications of this kind, accurate measurements of the shock pressure in water are needed for reliable assessment of results, particularly at very close range. Hantel and Davis[5] developed and calibrated a spherical shock-generating system using carefully manufactured explosive components, the main charge being composed of PBX 9205. The excellent reproducibility of their system would make it ideal for use at very close distances except that the cost of making the precision charges is prohibitively high for our use in explosive testing. (We have found that cast pentolite donor charges, made with reasonable care, give very good results.)

In the present work, the shock velocities, pressures, and pulse time histories in fresh water are measured as a function of distance from the pentolite

[1]Coleburn, N. L. and Roslund, L. A., "Interactions of Spherical Shock Waves in Water," Proceedings, Fifth Symposium on Detonation, 18-19 Aug 1970, pp. 581-588.

[2]Winning, C. H., "The Underwater Shock Wave Initiation of Cast Pentolite," in Proceedings of the Royal Society, Vol. 246, No. 1245, Jul 1958, pp. 288-296.

[3]Walker, F. E., and Wasley, R. J., "Initiation Patterns Produced in Explosives by Low-Pressure, Long-Duration Shock Waves," Combustion and Flame, Vol. 22, 1974, pp. 53-58.

[4]Liddiard, T. P., "The Initiation of Burning in High Explosives by Shock Waves," Proceedings, Fourth Symposium on Detonation, 12-15 Oct 1965, pp. 487-495.

[5]Hantel, L. W. and Davis, W. C., "Spherical Explosions in Water," Proceedings, Fifth Symposium on Detonation, 18-21 Oct 1970, pp. 599-604.

charge. The shock velocity as a function of distance is derived from framing and smear-camera records. The peak pressures and pulse time histories are measured using lithium niobate transducers. The pressure-vs-distance calibration, used in the earlier work of reference 4, was derived from shock velocities obtained from a relatively few framing-camera records. Since that work was done, many more data have been obtained and refinements have been made in analytical techniques.

As to pressures much farther away from the charge, tourmaline-gage measurements have been made of shock waves generated by large pentolite spheres under river or brackish water at distances greater than 12 charge radii. R. S. Price of NSWC summarizes the result with the expression

$$P = 2.46 \times 10^4 \, (W^{1/3}/R)^{1.194} \, , \qquad (1)$$

or

$$P = \frac{18.88}{(R/R_0)^{1.194}} \, , \qquad (1a)$$

where

P = peak pressure in pounds per square inch, Equation (1)

P = peak pressure in kilobars, Equation (1a)

W = charge weight in pounds

R = radial distance in feet

R_0 = charge radius.

The conversion of Equation (1) to (1a) is made using a density of 1.63 g/cm^3 for pentolite. Corrections for salinity and temperature variations are being made to the data on which Equation (1) is based so that an equation for shocks in fresh water for the large-scale tests will be available in the future.

The purpose of this report is to make available to others the data we have gathered from small-scale tests in fresh water and the equations that were developed which closely fit the data. The scalability of peak pressure and pulse widths as functions of relative radius, R/R_0, is a significant result. A useful analytical expression is presented which accurately reproduces the pressure-vs-R/R_0 data over the range of R/R_0 from 1.2 to 12.6. In the limit, $R/R_0 = 1$, it gives a pressure which agrees with the value obtained by Coleburn[6] using the Aquarium-Test technique.[7] In the limit $R/R_0 = \infty$, it gives zero

[6]Coleburn, N. L., Chapman-Jouget Pressures of Several Pure and Mixed Explosives, NOLTR 64-58, Jun 1964.

[7]Holton, W. C., The Detonation Pressure in Explosives as Measured by Transmitted Shocks into Water, NAVORD Report 3968, Dec 1954.

pressure. The shock pressures and time histories of shocks in water from pentolite spheres, calculated by Sternberg and Walker[8], are in fair agreement to the results of this study. Also there is reasonable agreement between their calculations, those of Rogers[9], and the far-field results given by Equation (1).

[8]Sternberg, H. M. and Walker, W. A., "Calculated Flow and Energy Distribution Following Underwater Detonation of a Pentolite Sphere," The Physics of Fluids, Vol. 14, No. 9, Sep 1971, pp. 1869-1878.

[9]Rogers, P. H., "Weak-Shock Solution for Underwater Explosive Shock Waves," Journal of the Acoustical Society of America, Vol. 62, 1977, pp. 1412-1419.

EXPERIMENTAL PROCEDURE

The shock velocity-versus-distance data contained in this report is derived mostly from Underwater Sensitivity Tests*, the experimental arrangement being shown in Figure 1. The spherical charge assembly is shown in Figure 2. The donor is an 82.2-mm diameter, cast pentolite sphere (50% TNT, 50% PETN), weighing 472 ± 2 g; density = 1.63 g/cm^3. The detonator is of the exploding bridgewire type, an RP-80, manufactured by Reynolds Industries, Inc. It is 7.11 mm in diameter and fits into a 46-mm deep hole cast into the sphere. A 7.0-mm diameter by 9.5 mm-long pellet (density = 1.6 g/cm^3) of pentolite is placed in the hole ahead of the detonator to ensure a rapid build-up to detonation in the main charge. The space around the detonator leads within the hole is filled with C-4 plastic explosive. A sealant is used to cover the connection of the plastic sheath, containing the detonator leads, to the pentolite sphere.

The shocks in water are observed by a Jacobs high-speed framing camera, described in Appendix A. The plane of focus is at right angles to the axis of the detonator. Diffuse, reflected back-lighting is provided by an argon explosive flashlamp which illuminates a white cardboard in back of the tank. (An exploding wire light source with a Fresnel lens also has been used to back-light the tank. However, the system is overly sensitive to minor disturbances in the water which tend to obscure the silouetted outlines of the acceptors.)

A calibration of the underwater system is obtained from the framing-camera records. For reasons of economy and expendiency, the Underwater Sensitivity Test experiments and a calibration of the system are carried out simultaneously. A typical sequence of frames is shown in Figure 3. The interframe time is 3.63 μs. (Two framing camera film strips are exposed in each shot, the frames of the two tracks being separated by 1.81 μs.) Not all of the records, or portions of records, are used in determining the calibration. On the records from some experiments, one or more acceptors are fairly close to the donor, thus limiting the number of x-t readings that are made in their direction. On other records, the degree of blur due to motion, or to being somewhat out of focus, is enough to eliminate all, or part, of the record from the calibration analysis. For the reasons given above, acceptable readings usually are obtained in only one or two of the four major directions on the record, i.e., toward the top, bottom, left, or right. Of these four directions, the first two usually produce the sharpest images on the film. As a result, only one record is included in the calibration with the snock-front image moving at right angles to the direction of slit motion.

*Sometimes called the Aquarium Test, but should not be confused with the underwater test of reference 7 from which detonation pressures are obtained.

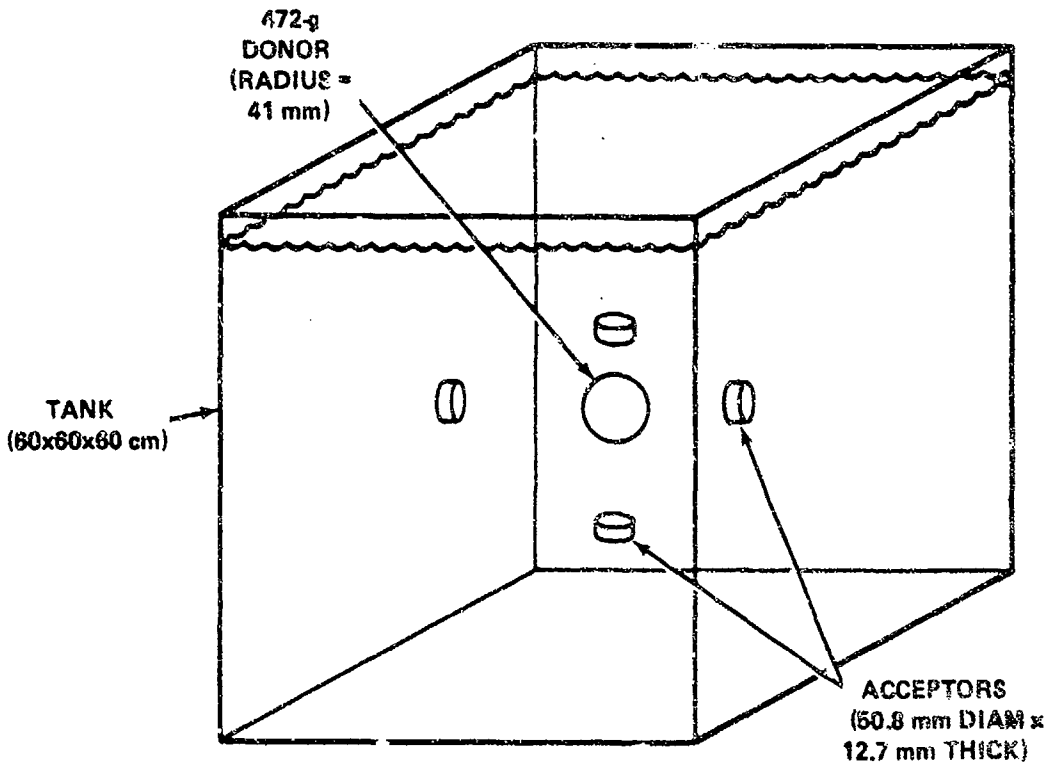

FIGURE 1. THE UNDERWATER SENSITIVITY TEST ARRANGEMENT

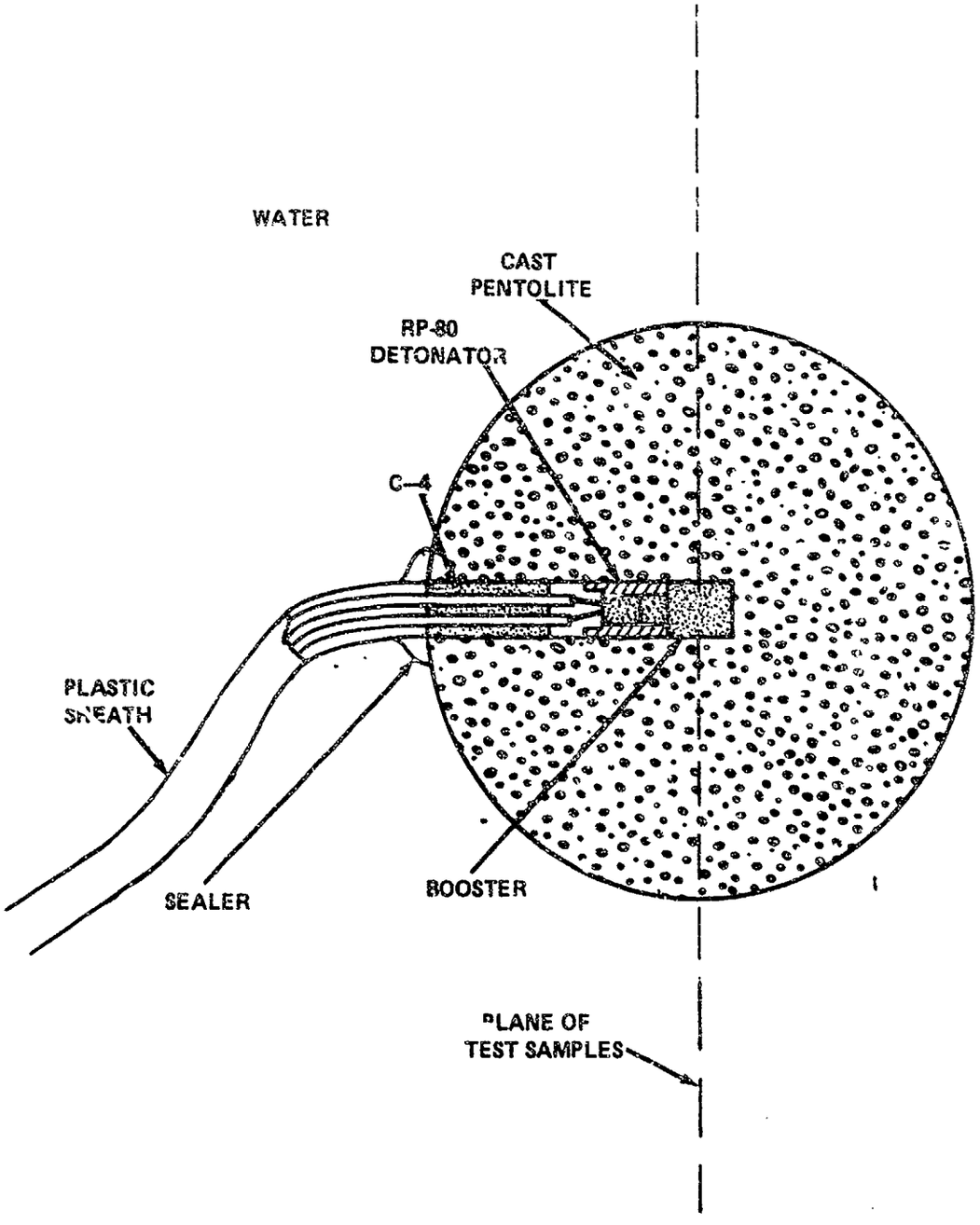

FIGURE 2. THE SPHERICAL CHARGE ASSEMBLY

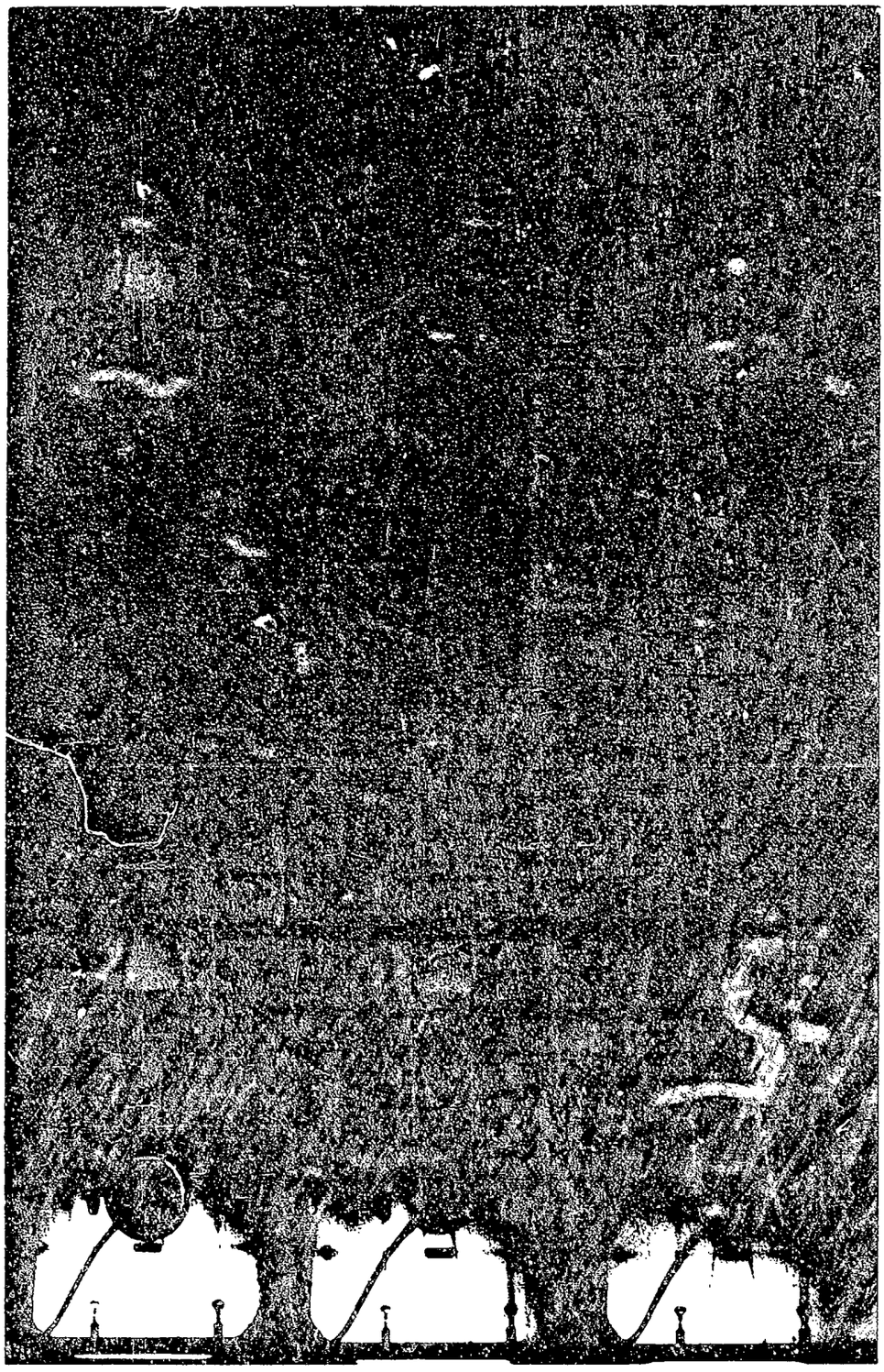

FIGURE 3. TYPICAL FRAMING CAMERA RECORD OBTAINED IN UNDERWATER SENSITIVITY TEST

The addition to photographic coverage, lithium niobate gages are used in some experiments to measure peak pressures and time histories at several distances from the pentolite sphere. The lithium niobate gage has the advantage of being made from commercially grown synthetic crystals and its calibration apparently is independent of manufacturer.[10]

The lithium niobate gage is used with capacitive loading as shown in Figure 4. The charge on the capacitor, generated by hydrostatic pressure, can be recorded by an oscilloscope. The lithium niobate hydrostatic piezoelectric constant of 6.3×10^{-8} coulomb/cm^2-kbar is used to convert charge to pressure. The oscilloscope input impedance must be large so that the discharge time of the capacitor through the scope impedance is small compared to the time of the event. Another consideration is to load the gage with a capacitance that is nearly 100 times that of the gage cable so that any changes in cable capacitance due to shock loading can be ignored.

Typical gage records are shown in Figure 5. There exists an extra oscillation superimposed on the voltage signal due to the pressure pulse. This extra signal is due to a normal mode oscillation of the lithium niobate crystal.[11] In reading the records, these normal mode oscillations are accounted for by drawing a line symmetrically through them. The peak pressure is determined by the intersection of the line through the normal mode oscillations and a projected line for the rise time of the pressure pulse.

[10] Graham, R. A., "Pressure Dependence of the Piezoelectric Polarization of $LiNbO_3$ and $LiTaO_3$," Ferroelectrics, Vol. 10, 1976, pp. 65-69.

[11] Goldstein, S., and Johnson, J. N., "Aquarium Tests on Aluminized ANFO," Pre-prints of the Seventh Symposium on Detonation, 16-19 Jun 1981, pp. 524-530.

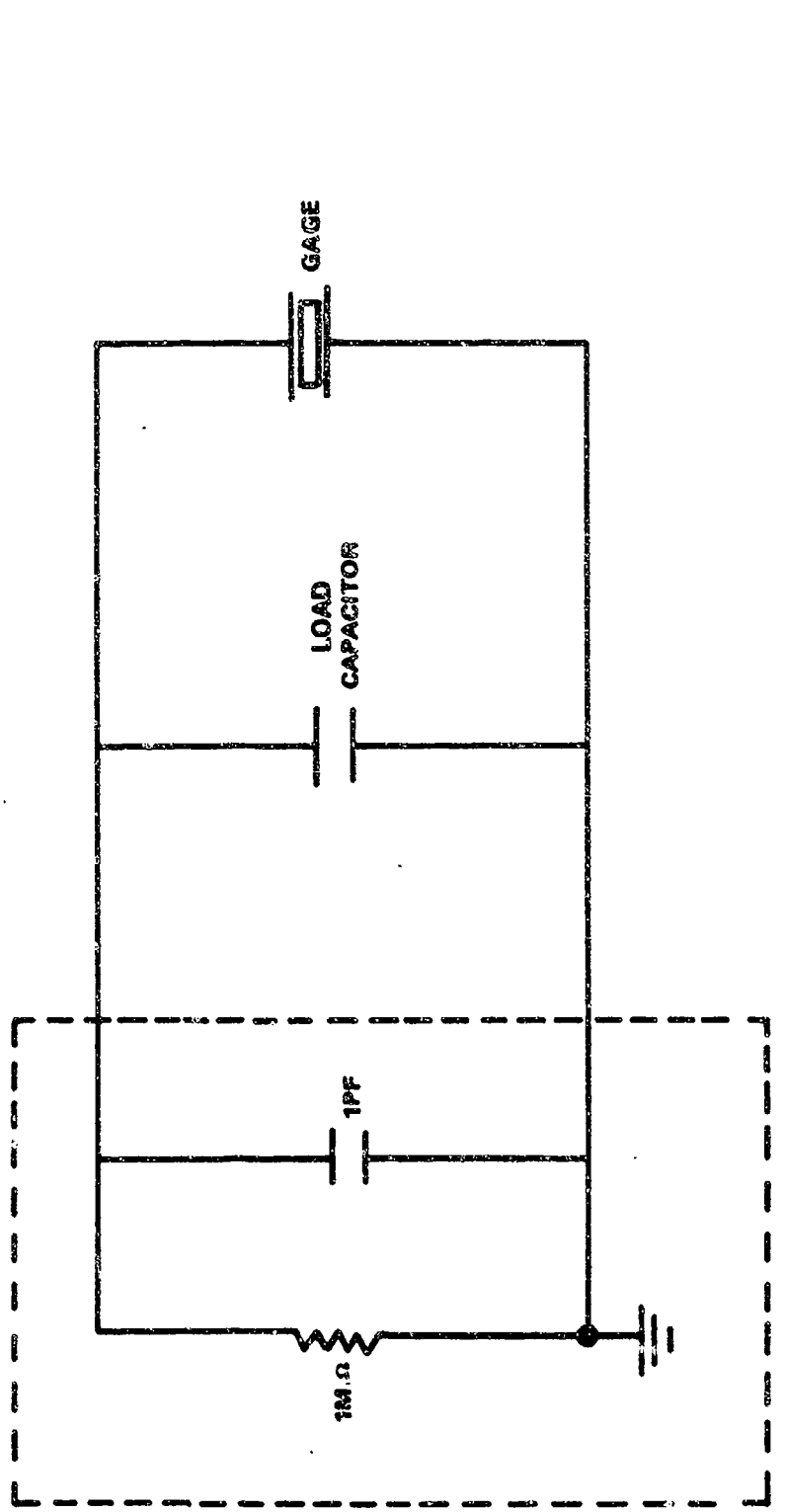

FIGURE 4. SCHEMATIC OF GAGE RECORDING CIRCUIT

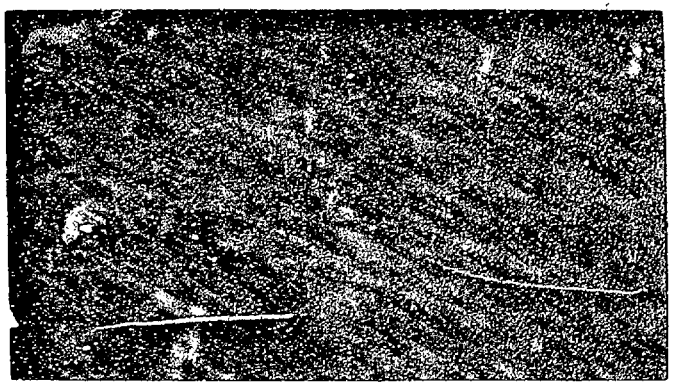

SHOT 2; R/R_o = 8.02
1V/DIV.; 10 μS/DIV.

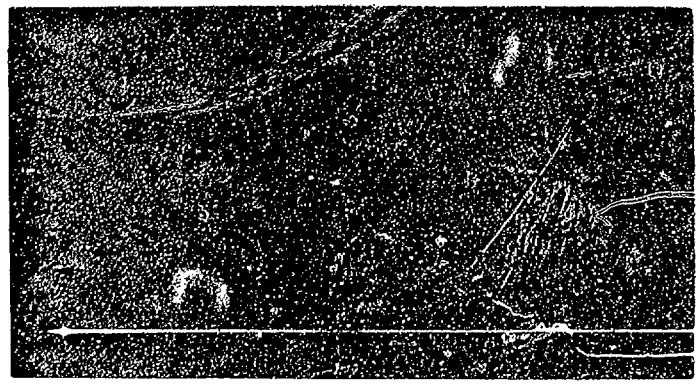

SHOT 4; R/R_o = 4.97
0.52V/DIV.; 20 μS/DIV.

SHOT 5; R/R_o = 8.01
0.057V/DIV.; 20 μS/DIV.

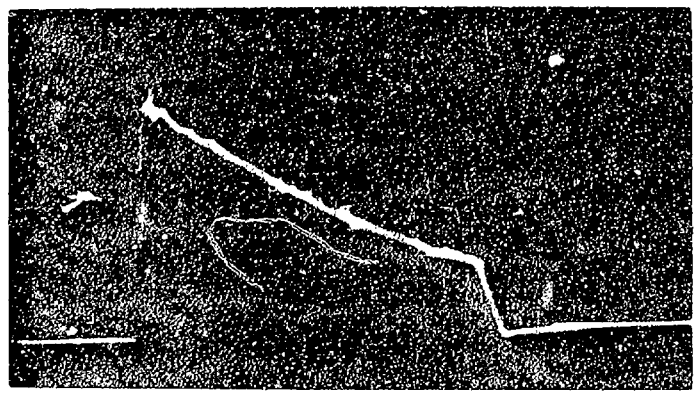

SHOT 6; R/R_o = 8.01
0.1V/DIV.; 20 μS/DIV.

FIGURE 5. PROFILES OF UNDERWATER SHOCK WAVES AS MEASURED BY LITHIUM NIOBATE GAGES

TREATMENT OF DATA

The pressure in the water, P, as a function of distance, x or R/R_0, is derived from experimentally determined values of the shock velocity as well as from pressure gages. The derivation from the shock velocity is made using the momentum relation, $P = \rho U_s u$, and the Rice-Walsh equation of state for water, $U_s = c_0 + 10.990 \ln(1 + u/51.9)$.[12] Combining the two equations results in

$$P = 51.9\ \rho U_s \left(\exp \frac{U_s - c_0}{10.990} - 1 \right) \qquad (2)$$

where

P = pressure (kbar)

U_s = shock velocity (mm/μs)

u = particle velocity (mm/μs)

c_0 = sound velocity (1.483 mm/μs)

ρ = density (0.998 g/cm^3).

To obtain shock velocities from the framing camera records, the x-t data are plotted, a smooth curve is drawn through the data, and the slopes are drawn at given values of x from 10 to 120 mm. However, before the x-t data are plotted certain corrections are made both in time and in distance (position). The position correction is a consequence of shock-front motion during the exposure time of the camera slits (focal plane shutters). If the velocity is constant, the position error is the same for all frames. However, any difference in shock velocity occurring between frames results in position errors that affect velocity calculations. For the detonated sphere the shock velocity initially is high, but rapidly decaying. This results in fairly large errors in position very close to the charge. The errors in position become relatively small a short distance away from the charge surface. A further discussion of correction due to motion blur is in Appendix A.

As to the time correction, the direction of shock motion on the film, relative to the camera slits, changes the interframe time if it is in the same

[12] Rice, M. H. and Walsh, J. M., "Equation of State of Water to 250 Kilobars," The Journal of Chemical Physics, Vol. 26, No. 4, Apr 1957, pp. 824-830.

direction as the slit motion, or if it opposes it. The time corrections are added if the slits and image are moving in the same direction and subtracted if they oppose each other. No time correction is necessary if the shock-front image motion is at right angles to the motion of the slits. This also is discussed in Appendix A. The uncorrected x-t data are found in Table A-1 and the corrected data in Table A-3 of Appendix A.

The shock-velocity data, Table 1, are derived from eight Underwater Sensitivity Test experiments, having 14 usable x-t framing camera sequences* over the range from x = 10 to 60 mm. Data for seven shots (13 sequences) are obtained from x = 10 to 70 or 80 mm, five shots (11 sequences) from x = 10 to 100 mm, and three shots (5 sequences) from x = 10 to 120 mm. In Table 1, two rows of instantaneous velocity values, U_s, are listed for each value of x. The upper row gives velocities obtained from all of the x-t sequences up to fourteen. The lower row gives the results from the eight individual experiments (shots). Where more than one x-t sequence is used per shot, the velocity values are averaged. The experimental values of the shock velocity (eight shots), U_s, the average deviation of the mean, a, and the number of measurements made are listed in Table 2 for various values of x and R/R_0. Two shock velocities obtained from smear-camera records also are included in Table 2. The peak pressures in the Table are obtained from Equation (2) and the experimental values listed for U_s.

The best fit to the data over the entire range is obtained using the following equation, the coefficients being determined by a least squares technique,

$$U_s - c_o = 4.57 \left(\frac{A + 1}{A + R_1^B} \right), \tag{3}$$

where

$$R_1 = R/R_0$$

$$A = -0.406213$$

$$B = 1.30135 .$$

This equation gives a limit of $U_s = 6.053$ mm/μs at $R_1 = 1$ which is adjusted to agree with the experimental value obtained by Coleburn[6] for 50/50 pentolite. Also, it converges to sonic velocity in the limit, $R_1 = \infty$. Several different expressions were tried before settling on Equation (3). The various expressions attempted and their fits to the data are presented in Appendix B.

*In eight shots with 16 film strips, the number of possible x-t sequences (up, down, left, and right) is 64.

TABLE 1. INSTANTANEOUS SHOCK VELOCITIES DERIVED FROM FOURTEEN FRAMING-CAMERA SEQUENCES (EIGHT SHOTS)

x-t SEQUENCE NUMBER	1	2	3	4	5	6	7	8	9	10	11	12	13	14
SHOT NUMBER	JK-006		-008		-009		-010	-011				-012	-015	-017
DIRECTION OF SHOCK PROPAGATION	DOWN		DOWN	UP	UP		LEFT	UP		DOWN		UP	UP	UP
TRACK	A	B	A	A	A	B	A	A	B	A	B	A	A	A

x (mm)	SHOCK VELOCITY (mm/μs)												MEAN	σ
10	4.27	4.35	4.37	4.40	4.46	4.76	4.65	4.49	4.54	4.29	4.53	4.24	4.424	0.127
	4.310		4.385		4.610		4.65	4.463				4.24	4.405	0.127
20	3.58	3.65	3.69	3.64	3.65	3.97	3.65	3.80	3.83	3.68	3.70	3.59	3.681	0.083
	3.615		3.665		3.810		3.65	3.753				3.59	3.649	0.070
30	3.15	3.18	3.20	3.18	3.13	3.29	3.13	3.18	3.26	3.19	3.20	3.21	3.178	0.041
	3.165		3.190		3.160		3.13	3.208				3.21	3.157	0.038
40	2.90	2.83	2.86	2.83	2.83	2.82	2.78	2.85	2.89	2.89	2.84	2.85	2.841	0.028
	2.865		2.845		2.825		2.78	2.868				2.85	2.829	0.028
50	2.64	2.60	2.60	2.60	2.63	2.56	2.60	2.55	2.61	2.63	2.61	2.61	2.599	0.021
	2.620		2.600		2.595		2.60	2.600				2.61	2.596	0.014
60	2.45	2.40	2.48	2.44	2.43	2.42	2.43	2.40	2.44	2.45	2.45	2.48	2.435	0.021
	2.430		2.460		2.425		2.43	2.435				2.48	2.434	0.019
70	2.34	2.30	2.36	2.32	2.28	2.30	2.29	2.30	2.30	2.34	2.38	2.35	2.317	0.029
	2.320		2.340		2.290		2.29	2.330				2.35	2.311	0.027
80	2.24	2.17	2.25	2.24	2.17	2.20	2.23	2.20	2.18	2.25	2.26	2.24	2.218	0.029
	2.205		2.245		2.185		2.23	2.223				2.24	2.218	0.019
100	2.07	2.11	2.09	2.05	2.07	2.08	2.07	2.10	2.12	2.06	2.18	-	2.091	0.027
	2.090		2.070		2.075		2.07	2.115			-	-	2.084	0.015
120	1.97	-	1.99	1.97	1.96	1.99	-	-	-	-	-	-	1.976	0.011
	1.97	-	1.980		1.975		-	-	-	-	-	-	1.975	0.005

TABLE 2. SUMMARY OF THE MEASURED INSTANTANEOUS SHOCK VELOCITIES AND THE CORRESPONDING PRESSURES OBTAINED FROM EQUATION (2)

x (mm)	R/R_o	NUMBER MEASURED	U_s (mm/μs)	AV. DEV. OF MEAN	P (kbar)[a]
10	1.243	8	4.405	0.127	69.5
20	1.487	8	3.649	0.070	41.2
30	1.730	8	3.157	0.038	26.9
40	1.973	8	2.829	0.028	19.1
50	2.217	8	2.596	0.014	14.3
60	2.460	8	2.434	0.019	11.4
70	2.703	7	2.311	0.027	9.4
80	2.946	7	2.218	0.019	8.0
100	3.433	5	2.084	0.015	6.1
120	3.920	3	1.975	0.005	4.7
89	8.02[b]	1	1.686[c]	0.03	1.63
143	12.27[b]	1	1.583[c]	0.02	0.75

[a]From Equation (2)

[b]R_o = 12.7 mm, all others are 41.1 mm

[c]Smear-camera measurements of shock velocity; the other velocities listed are from Jacobs framing-camera records. Gage measurements also were made in these two experiments.

The peak pressures and pulse half-widths are measured by lithium niobate gages for a number of cast and pressed pentolite spheres with radii of 1.27, 4.11, and 6.84 cm. Information on the spheres is given in Table 3. The peak pressure and pulse widths at one-half peak pressure are given in Table 4. The measured pressures span a range of 0.8 to 5.9 kbar for a relative distance, R/R_0, from 12.3 to 3.5, respectively. The peak pressures for the same R/R_0 in Table 4 are the same within experimental error. The pulse half-widths ranged from 10 to 66 μs. The pulse half-widths divided by R_0 give the same results for the different size spheres when the measurements are made at the same R/R_0. The one exception in Table 4 is for τ/R_0 = 11.73 μs/cm at R/R_0 = 8.01. No adequate explanation exists for its departure from the noted trend.

TABLE 3. PENTOLITE SPHERE AND LITHIUM NIOBATE GAGE SPECIFICATIONS

SHOT NO.	GAGE NO.	CHARGE RAD. (cm)	DENSITY (g/cm^3)	GAGE CAP.[a] ($10^{-9}F$)	TOTAL CAP. ($10^{-9}F$)	GAGE DIST.[c] (cm)
1	1	1.27	1.61[b]	0.45	10.3	15.56
2	1	1.27	1.62[b]	0.45	10.3	10.16
3	1	4.11	1.65	--	40.0	18.06
4	1	4.11	1.64	--	79.0	14.26
4	2	4.11	1.64	--	40.0	20.41
5	1	4.11	1.62	1.5	121.0	32.94
5	2	4.11	1.62	1.5	81.0	50.47
6	1	6.84	1.62	~2.0	121.0	44.49
6	2	6.84	1.62	~2.0	81.0	54.82

[a]Includes capacitance of cable

[b]Pressed

[c]From center of sphere

TABLE 4. GAGE MEASUREMENTS OF SHOCKS FROM THREE SIZES OF PENTOLITE SPHERES

SHOT NO.	R/R_o	PEAK PRESSURE (kbar)	τ, PULSE HALF-WIDTH (μs)	τ/R_o (μs/cm)	WATER TEMP. (°C)
1	12.27	0.803 ± 0.030	15.23 ± 0.61	12.01 ± 0.48	21.1
2	8.02	1.447 ± 0.043	12.46 ± 0.93	9.83 ± 0.58	22.2
3	4.39	3.823 ± 0.126	24.56 ± 0.85	5.98 ± 0.21	17.8
4	3.47	5.862 ± 0.251	10.32 ± 1.93	2.51 ± 0.47	17.8
4	4.97	3.048 ± 0.080	24.66 ± 1.16	6.00 ± 0.28	17.8
5	8.01	1.543 ± 0.076	48.19 ± 2.96	11.73 ± 0.72	20.6
5	12.28	0.817 ± 0.033	50.08 ± 2.42	12.18 ± 0.59	20.6
6	6.50	2.038 ± 0.075	57.15 ± 2.87	8.36 ± 0.42	26.0
6	8.01	1.449 ± 0.061	65.88 ± 1.48	9.63 ± 0.22	26.0

DISCUSSION

A useful form of the data is in terms of peak pressure as a function of distance in water from the pentolite sphere. Combining Equation (3) with Equation (2) results in

$$P = 76.814 \left[1 + \frac{1.8298}{R_1^{1.3014} - 0.4062}\right] \left[\exp\left(\frac{0.2469}{R_1^{1.3014} - 0.4062}\right) - 1\right] \qquad (4)$$

where

P = peak pressure in kilobars

R_1 = relative distance, R/R_0, from 1.24 to 14.3.

The coefficients given here differ somewhat from those given in reference 13. The change is due to the inclusion of more refined x-t data and velocity measurements in the later calculations. In Figure 6, the solid line gives the peak pressure as a function of R/R_0 as obtained from Equation (4). The lithium niobate data, shown as bars, are in good agreement with the solid line. The dashed line in Figure 6, representing Equation (1) is in fair agreement with the data for pressures below five kilobars. Note that Equation (4) predicts pressures slightly lower than Equation (1) for large values of R_1, i.e., $R/R_0 > 10$. For the most part, the small differences in the predicted results from these two equations for large R/R_0 are likely to be due to gage inaccuracies and to Equation (1) being based on data from large-scale field tests in brackish water with variations in temperature. The pressure calculated from the measured shock velocity at $R/R_0 = 8.02$ in Table 2 is 11% higher than the gage measurement listed in Table 4 for the same experiment. A velocity of only 1% lower than shown, however, results in a pressure that agrees with the corresponding gage measurement to within experimental error.

The measured pulse half-widths as a function of R/R_0 are given in Figure 7. The gage pulse width data are in fair agreement with the calculated results, the measured pulse half-widths being higher than the code calculation for R/R_0 values greater than seven. For R/R_0 less than five, the measured half-widths are less than calculated. The record at 3.5 has a structure to it which other records did not show. It is possible that this gage was breaking under high loading. This possibility is further supported by the fact that a gage at $R/R_0 = 1.89$ gave no record (not included in Table 4) and we suspect that its elastic yield

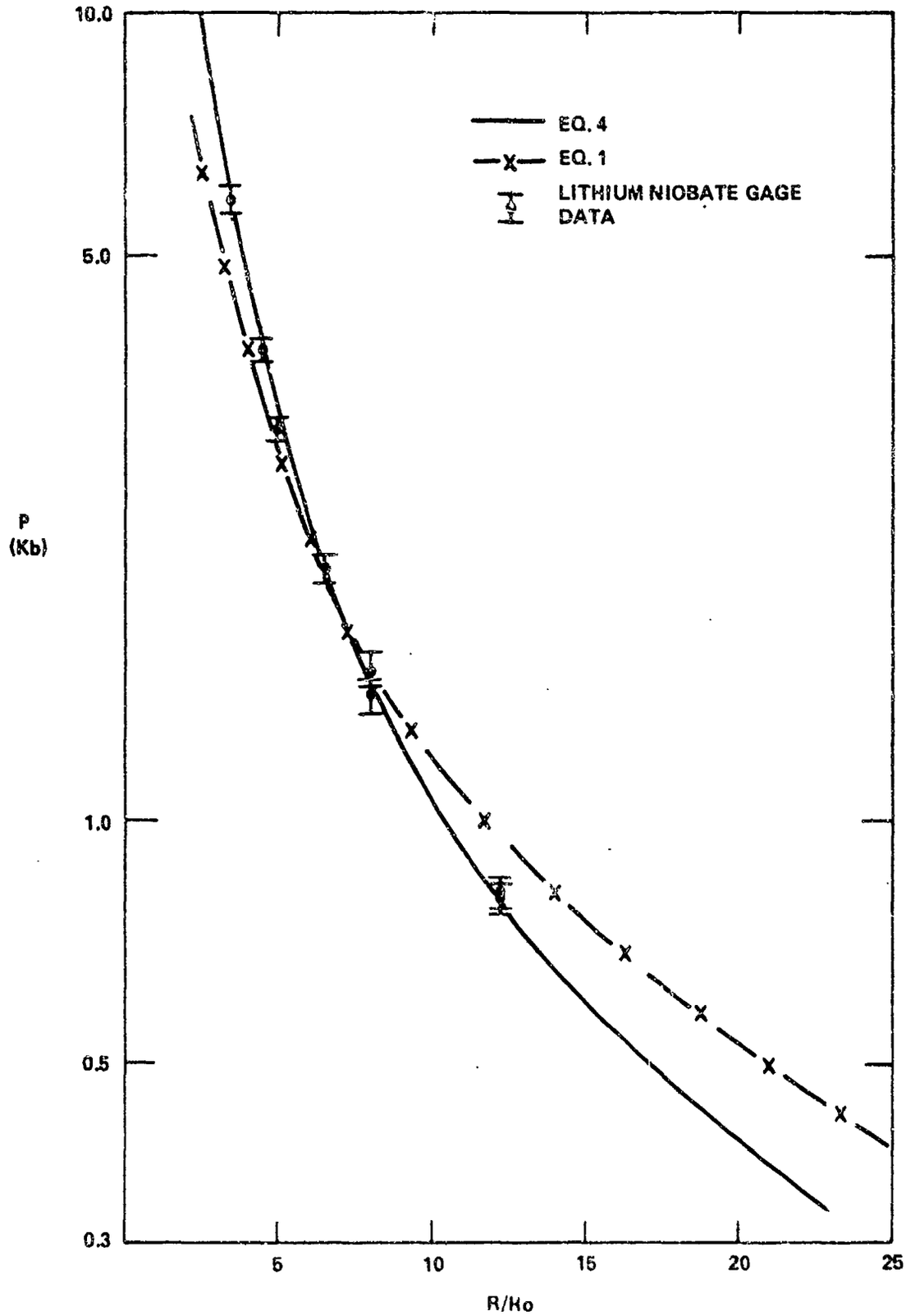

FIGURE 6. PEAK PRESSURE VERSUS RELATIVE DISTANCE FROM PENTOLITE SPHERES

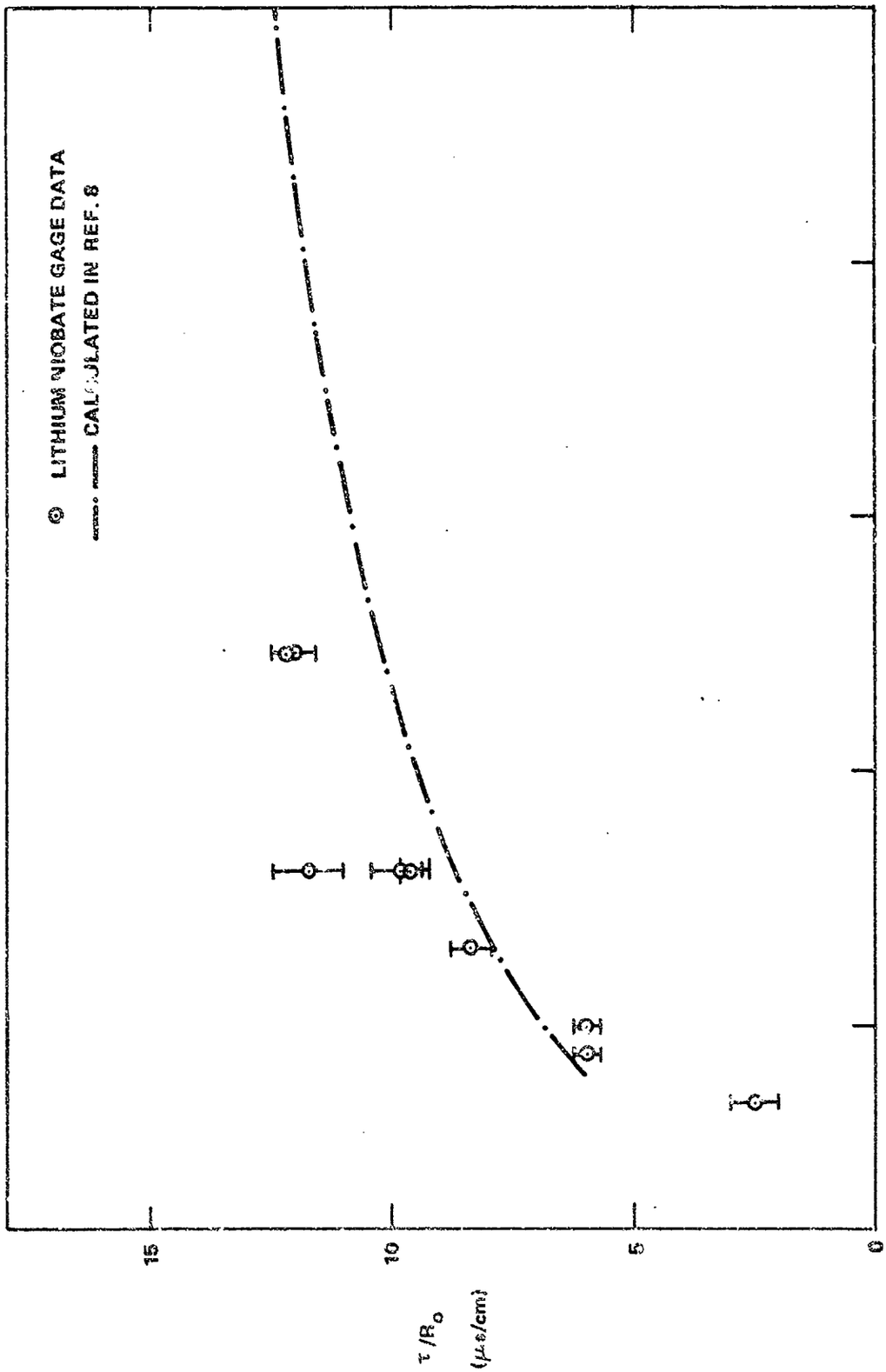

FIGURE 7. SCALED PULSE WIDTHS AT ONE-HALF PEAK PRESSURE

point was exceeded causing irreversible damage to the crystal. The trend in the data is in agreement with the hydrodynamic code calculations.[8]

Shock data for distances greater than $R/R_0 = 12$ are of secondary interest to this work. However, to make this a more complete report, the work of Sternberg and Walker[8] and that of Rogers[9] will be briefly discussed. The hydrodynamic code calculations by Sternberg and Walker[8] are in good agreement with the field-test data represented by Equation (1). The paper by Rogers[9] successfully derives an analytical expression for peak pressure and pulse width for exponentially decaying shocks as a function of distance from the charge. To use these expressions requires knowing the shock-pulse amplitude and width at one position. The theory then predicts the pulse amplitude and width at later times and positions. This theory was not expected to give accurate results for shock pressures of greater than about two kilobars. In Appendix C are shown the results of fitting the peak pressures and time-pulse widths obtained in this study to the analytical expressions derived by Rogers.

CONCLUSIONS

Shock wave velocities, peak pressures and pulse widths at one-half peak pressure have been measured as a function of distance in fresh water from pentolite spheres. An analytic function that reproduces the pressure data within experimental error over the relative distance (R/R_0) interval from 1.2 to 12 has been found. This expression is empirical and results from the observation that the shock velocity minus the sound velocity is proportional to $1/(R^B + A)$. The pressure equation goes to the desired limits of 162 kbar at $R/R_0 = 1$ (the experimental value determined by Coleburn) and 0 kbar at $R/R_0 = \infty$. The measured peak pressures agree within experimental error with Equation (4).

The calculated shock pressures and time histories of shocks in water from pentolite spheres by Walker and Sternberg are in fair agreement with the present experimental results. Extrapolation of the present data by Equation (4) to $R/R_0 > 13$ results in pressures slightly lower than measure in large-scale field tests.

The pressure pulse in water from the pentolite sphere can be scaled as a function of the sphere radius. This indicates that most or all of the pentolite detonates even for very small spheres of 1.27 cm radius. This is consistent with the known short run distance to detonation for pentolite.

REFERENCES

1. Coleburn, N. L. and Roslund, L. A., "Interactions of Spherical Shock Waves in Water," Proceedings, Fifth Symposium on Detonation, 18-19 Aug 1970, pp. 581-588.

2. Winning, C. H., "The Underwater Shock-Wave Initiation of Cast Pentolite," in Proceedings of the Royal Society, Vol. 246, No. 1245, Jul 1958, pp. 288-296.

3. Walker, F. E., and Wasley, R. J., "Initiation Patterns Produced in Explosives by Low-Pressure, Long-Duration Shock Waves," Combustion and Flame, Vol. 22, 1974, pp. 53-58.

4. Liddiard, T. P., "The Initiation of Burning in High Explosives by Shock Waves," Proceedings, Fourth Symposium on Detonation, 12-15 Oct 1965, pp. 487-495.

5. Hantel, L. W. and Davis, W. C., "Spherical Explosions in Water," Proceedings, Fifth Symposium on Detonation, 18-21 Oct 1970, pp. 599-604.

6. Coleburn, N. L., Chapman-Jouget Pressures of Several Pure and Mixed Explosives, NOLTR 64-58, Jun 1964.

7. Holton, W. C., The Detonation Pressure in Explosives as Measured by Transmitted Shocks into Water, NAVORD Report 3968, Dec 1954.

8. Sternberg, H. M. and Walker, W. A., "Calculated Flow and Energy Distribution Following Underwater Detonation of a Pentolite Sphere," The Physics of Fluids, Vol. 14, No. 9, Sep 1971, pp. 1869-1878.

9. Rogers, P. H., "Weak-Shock Solution for Underwater Explosive Shock Waves," Journal of the Acoustical Society of America, Vol. 62, 1977, pp. 1412-1419.

10. Graham, R. A., "Pressure Dependence of the Piezoelectric Polarization of $LiNbO_3$ and $LiTaO_3$," Ferroelectrics, Vol. 10, 1976, pp. 65-69.

11. Goldstein, S., and Johnson, J. N., "Aquarium Tests on Aluminized ANFO," Proceedings, Seventh Symposium on Detonation, 16-19 Jun 1981, pp. 1016-1023.

12. Rice, M. H. and Walsh, J. M., "Equation of State of Water to 250 Kilobars," The Journal of Chemical Physics, Vol. 26, No. 4, Apr 1957, pp. 824-830.

REFERENCES (CONT.)

13. Liddiard, T. P. and Forbes, J. W., "Shock Waves in Fresh Water Generated by Detonation of Pentolite Spheres," Proceedings of the A.P.S. Topical Conference on Shock Waves in Condensed Matter, Menlo Park, CA, Jun 1981, pp. 578-582.

APPENDIX A

CORRECTION OF DISTANCE-TIME DATA DERIVED FROM JACOBS CAMERA RECORDS

THE JACOBS CAMERA

The Jacobs camera records a total of six rows of 24 x 18 mm pictures, three rows on each of two 70 mm film tracks. A maximum of 216 pictures are available. In a focal plane shutter camera only a narrow band of the frame is exposed by the moving aperture (a slit in this case) at a single instant of time. Ultimately the entire field of view is scanned as the slit moves across the whole frame. In this camera six pictures are partially exposed simultaneously (one per row) through six slits, the slits being displaced one-sixth of a frame apart. Thus, for the duration of the recording portion of the camera's duty cycle, the field is continuously scanned by six narrow bands over and over again, each scan by each band exposing a separate picture. The shutter action is illustrated in Figure A-1.

In this camera time on the film track increases in two modes, between frames and within frames. Within a single frame the focal plane shutter (actually the 1 : 1 image of the slit) sweeps across the frame area exposing the film one slit width at a time. The slit widths can be set in either track at 0.002, 0.005, 0.010, 0.020, 0.040, and 0.080 inch. At a rotating mirror speed of 300 rps the focal plane shutter sweep velocity is 2.298 mm/μs. (This is the speed used throughout the Underwater Sensitivity Test experiments.) Thus, time within a frame increases at a rate of 0.435 μs/mm. At this rate the slit traverses the 25 mm distance, from a point in one frame to the corresponding point in the next frame, in 10.88 μs. This is the interframe time for horizontally adjacent images. Since these shutters move simultaneously along each track, phased one-sixth of a frame apart, time advances by 3.628 μs between frames in all three rows in each track and 1.814 μs, alternating between frames in both tracks. For further details concerning the Jacobs camera, see reference A-1.

CORRECTIONS FOR MOTION BLUR

In reading the framing camera records, the shock-front image position on the film, including the motion blur, $\Delta x'$, is denoted by $x' + \Delta x'$. The position correction, however, is made after the original readings are converted to full scale, i.e., they are divided by the magnification factor (actually a reduction factor), M, giving values of $x + \Delta x$. The real (corrected) shock-front position, x, is obtained by subtracting out Δx, after Δx has been determined. The

---

A-1 Jacobs, S. J., McLanahan, J. D., Jr., and Whitman, E. C., "A High-speed Focal-Plane Shutter Framing Camera," Journal of the Society of Motion Picture and Television Engineers, Vol. 72 No. 12, Dec 1963, pp. 923-926.

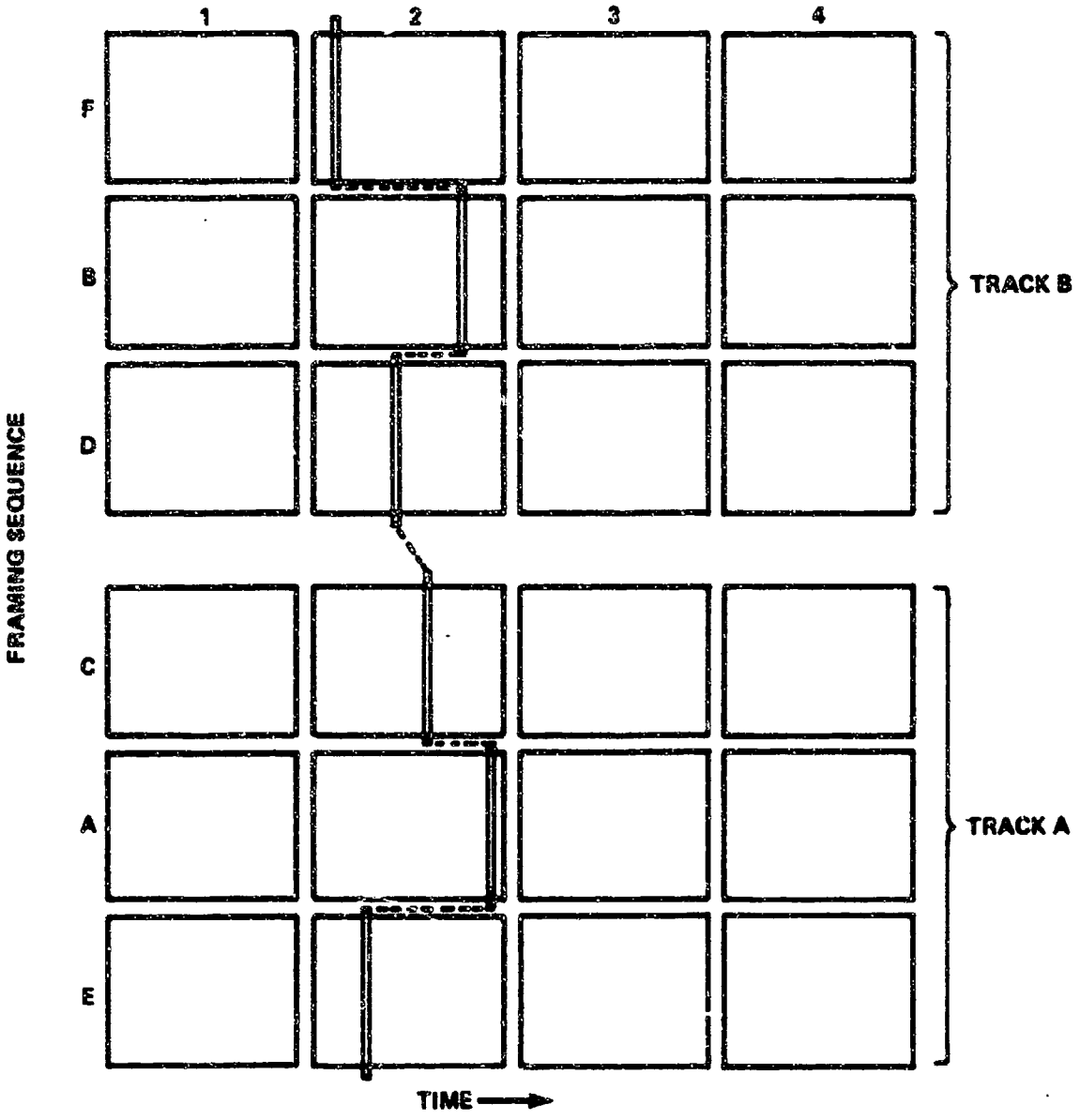

FIGURE A-1. SEQUENCE OF FRAMES FORMED BY SIX FOCAL PLANE SHUTTERS WRITING IN TRACKS A AND B

uncorrected readings of $x' + \Delta x'$ from the records are given in Table A-1 for fourteen sequences, along with the corresponding (full scale) values of $x + \Delta x$. In most cases, M can be considered constant throughout the sequence. However, in a few cases M changes gradually over the distance being read over the record. For the most part, this is due to some tilt of a mirror placed in the optical path within the firing chamber to give a greater distance to the object. The image of a graduated scale on the film, in the plane of focus within the tank, permits a check of the constancy of the magnification factor. The values of M used are not listed in the Table, but can be determined by dividing $x + \Delta x$ by $x' + \Delta x'$.

How a correction is made for image motion blur depends on the direction taken by the point being followed on the shock-front image. For a slit width, W, and a slit velocity, U_f, the correction for image blur, $\Delta x'$, is different for each of the three following conditions: Case 1, when the shock-front image motion is in the same direction as the slit motion, i.e., downward; Case 2, when the shock-front motion is in the opposite, upward direction; and Case 3, when the shock-front motion is at right angles to the direction of slit motion.

In Case 1, shock and slit in the same direction, the effective slit width is $W + \Delta x'$, $\Delta x'$ being the amount of blur on the film and is incorporated in the distance value read from the framing camera, i.e., $x' + \Delta x'$. This is illustrated on the right side of Figure A-2. At $t = t_1$ the shock-front image just overtakes the leading edge of the slit image, A_1. The exposure of the film lasts until the back of the slit, B_1, overtakes the shock-front image at $t = t_2$ (position B_2 in the sketch.) At the instant the shock-front image is cut off, the leading edge of the slit has moved from A_1 to A_2 or a distance equal to the slit width, W, plus the motion blur, $\Delta x'$. Thus, the exposure time of the moving shock-front image, τ, is $(W + \Delta x')/U_f$. In Case 2, with shock and slit moving in opposing directions, the effective slit width is $W - \Delta x'$. This can be deduced from the slit and shock-front positions shown at the left side of Figure A-2. (Note that, in reality, the image of the expanding shock front cannot be a true circle and t_1 cannot have the same value for all three cases on the record. The shock fronts are drawn spherically here for simplicity and this in no way affects the results when each case is considered separately.) It can be shown that τ' also is equal to $\Delta x'/(M \cdot \bar{U}_s)$, $\bar{U}_s$ being the average velocity of the shock-front image across the effective slit width. Therefore, $\tau' = (W \pm \Delta x')/U_f = \Delta x'/(M \cdot \bar{U}_s)$. Solving for blur on the film,

$$\Delta x' = \frac{W \cdot M \cdot \bar{U}_s}{U_f \pm M \cdot \bar{U}_s} ,$$

where the sign in the denominator is minus when U_f and $M \cdot \bar{U}_s$ move in the same direction and positive when they move in opposition. It follows then that the full-scale (object) motion blur is

$$\Delta x = \frac{\Delta x'}{M} = \frac{W \cdot \bar{U}_s}{U_f \pm M \cdot \bar{U}_s} \qquad \text{(A-1)}$$

TABLE A-1. UNCORRECTED x-t DATA FROM EIGHT EXPERIMENTS HAVING FOURTEEN USABLE SEQUENCES ($x' \pm \Delta x'$ and $x \pm \Delta x$ in mm)

	SEQUENCE 1		2		3		4		5		6		7	
t' (μs)	$x' \pm \Delta x'$	$x \pm \Delta x$	$x' \pm \Delta x'$	$x \pm \Delta x$	$x' \pm \Delta x'$	$x \pm \Delta x$	$x' \pm \Delta x'$	$x \pm \Delta x$	$x' \pm \Delta x'$	$x \pm \Delta x$	$x' \pm \Delta x'$	$x \pm x\Delta$	$x' \pm \Delta x'$	$x \pm \Delta x$
3.63	0.50	12.6	-	-	0.57	14.2	0.25	6.3	0.43	11.0	0.13	3.3	0.58	14.8
7.26	1.03	25.9	0.83	20.8	1.11	27.7	0.78	19.8	0.93	23.9	0.68	17.4	1.10	28.0
10.88	1.51	38.0	1.32	33.2	1.60	39.9	1.25	31.8	1.35	34.7	1.18	30.3	1.52	38.7
14.51	1.94	48.8	1.78	44.7	2.01	50.0	1.64	41.7	1.74	44.7	1.58	40.5	1.91	48.7
18.14	2.31	58.1	2.19	55.0	2.40	59.7	1.99	50.7	2.10	53.9	1.94	49.7	2.27	57.8
21.77	2.69	67.6	2.53	63.6	2.78	69.1	2.35	59.9	2.43	62.4	2.28	58.5	2.62	66.7
25.39	3.05	76.7	2.89	72.6	3.15	78.2	2.68	68.3	2.74	70.4	2.60	66.7	2.95	75.1
29.02	3.36	84.5	3.21	80.7	3.48	86.4	2.98	76.0	3.05	78.3	2.92	74.9	3.25	82.8
32.65	3.70	93.0	3.55	89.2	3.80	94.3	3.29	84.0	3.34	85.8	3.22	82.6	3.56	90.7
36.28	4.02	100.9	3.86	97.0	4.12	102.1	3.59	91.7	3.64	93.5	3.52	90.3	3.88	98.8
39.91	4.30	108.1	4.17	104.8	4.43	109.8	3.86	98.7	3.93	100.9	3.80	97.4	4.16	106.0
43.53	4.61	115.7	4.47	112.3	4.75	117.6	4.15	106.1	4.20	107.9	4.08	104.6	4.44	113.1
47.16	4.92	123.5	4.77	119.9	5.05	125.0	4.42	113.1	4.45	114.8	4.36	111.8	-	-
50.79	-	-	-	-	-	-	4.69	120.1	4.74	121.7	4.63	118.7	-	-
54.42	-	-	-	-	-	-	4.97	127.3	-	-	4.89	125.4	-	-

	SEQUENCE 8		9		10		11		12		13		14	
3.63	0.55	14.2	0.22	5.6	0.30	7.7	0.57	14.7	0.33	7.9	0.21	5.2	0.53	13.4
7.26	1.05	27.0	0.78	20.0	0.89	22.9	1.10	28.3	0.88	20.9	0.76	18.8	1.03	25.8
10.88	1.48	38.1	1.25	32.0	1.39	35.8	1.58	40.6	1.37	32.6	1.22	30.2	1.46	36.5
14.51	1.87	48.1	1.66	42.5	1.81	46.6	2.00	51.4	1.79	42.6	1.64	40.6	1.82	45.7
18.14	2.20	56.6	2.02	51.7	2.19	56.3	2.38	61.2	2.18	51.8	1.99	49.3	2.20	55.1
21.77	2.52	64.8	2.35	60.2	2.56	65.9	2.70	69.4	2.55	60.6	2.35	58.2	2.51	62.8
25.39	2.83	72.8	2.67	68.4	2.88	74.1	3.06	78.7	2.91	69.2	2.68	66.4	2.83	71.0
29.02	3.13	80.5	2.98	76.3	3.21	82.6	3.39	87.2	3.25	77.3	-	-	3.15	79.0
32.65	3.43	88.3	3.29	84.2	3.55	91.3	3.69	94.9	3.57	84.9	-	-	3.46	86.7
36.28	3.72	95.7	3.59	91.9	3.85	99.1	4.00	102.8	-	-	-	-	-	-
39.91	4.01	103.2	3.87	99.1	4.14	106.5	-	-	-	-	-	-	-	-
43.53	-	-	4.14	105.6	-	-	-	-	-	-	-	-	-	-

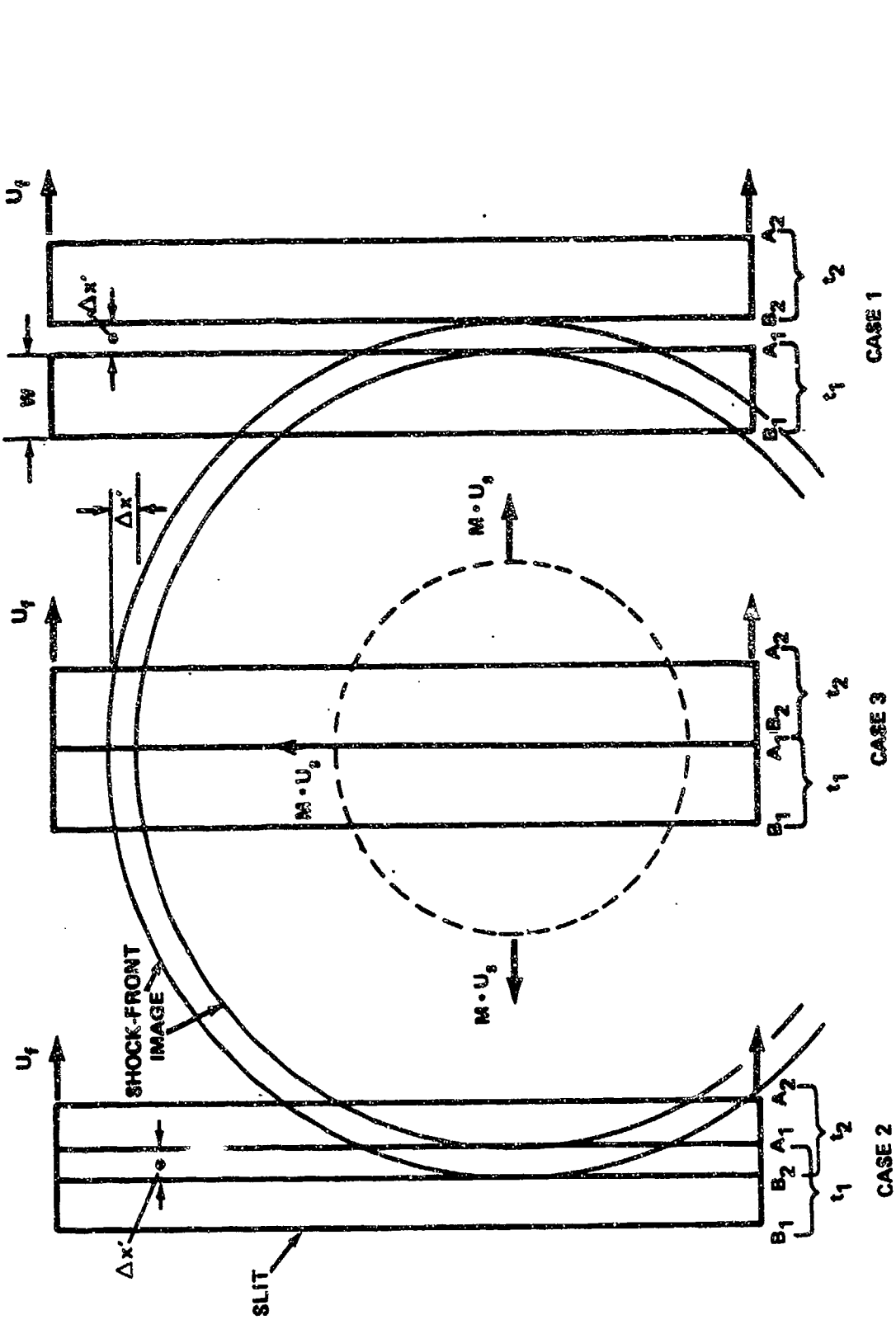

FIGURE A-2. IMAGE BLUR CAUSED BY SHOCK-FRONT MOTION IN THREE DIRECTIONS RELATIVE TO THE SLIT MOTION

In Case 3, with the shock-front image motion at right angles to the direction of slit motion, the exposure time is taken to be equal to the slit duration. This is indicated in the center of Figure A-2. The slit duration is defined here as the time it takes the slit to travel its own width, i.e., W/U_f. The motion blur on the film, $\Delta x'$, is defined as $(M \cdot W)/\bar{U}_s$ in this case, and the object motion blur, Δx, is $W/\bar{U}_s$.

In determining the correction curve, a series of values of x (the true, full-scale, shock-front position) are chosen at convenient intervals from 0 to 120 mm. The required values of $\bar{U}_s$ are determined in the following way. First, the instantaneous shock velocity, U_s, is found for each value of x selected, using Equation (3). The values of U_s corresponding to the true position, x, are listed in the first two columns of Table A-2. An approximate value of Δx for Cases 1 or 2 is obtained by substituting U_s for $\bar{U}_s$ in Equation (A-1). The value of M used here is 25.3, the mean value of all x-t sequences. (Actually, one could use any value of M from 24 to 26 without affecting the results appreciably.) In Case 3, the substitution is made in the expression $\Delta x = w/\bar{U}_s$. The approximate values of Δx, so determined, are added to x and U_s is calculated at that position. The mean between the two values at x and $x + \Delta x$ is used to determine a more refined value of Δx. The process is repeated to obtain the final value of $\bar{U}_s$ and Δx given in Table A-2. The resulting correction curves for five combinations of two slit widths and three directions of slit motion are shown in Figure A-3. Using corrections taken from the curves, the uncorrected data in Table A-1, $x' + \Delta x'$ for the image and $x + \Delta x$ for full scale, are converted to the corrected distance, x, given in Table A-3. The corrected time, t, also is included and is discussed next.

CORRECTIONS FOR TIME

After the values of x', i.e., x/M, are determined, the correction for time, Δt, can be made simply by dividing x' by the slit velocity, U_f (2.298 mm/μs), i.e., $\Delta t = x'/U_f$. If the shock front and slits are moving in the same direction, Δt is added to the accumulated time, t'. In each track the uncorrected time, t', increases by 10.883 μs per frame along a row and by 3.628 μs when taking into account both rows and columns. If the direction of shock motion is in opposition to the slit, Δt is subtracted from t'. There is no correction when the shock motion is at right angles to the slit motion. The derivation of the time correction, Δt, can be demonstrated by Figure A-4. Three consecutive frames, running parallel to the film edge, are shown (upper row) in which an element of the shock-front image is advancing in the same direction as the focal plane shutter. The position of the shock-front element in the first frame is taken as zero reference, (t_0, x_0). The primes added to t_0 in succeeding frames denote zero time plus accumulated interframe times. The resulting reference time lines, t_0, t_0' and t_0'', are in the same relative position, x_0, within each frame. It is seen that in order for the shock front to be exposed in the next frame, the slit must move from a position, x_0, to x_1 which lies to the right of the reference time line, t_0'. This means that, in effect, the time between frames increases as far as the shock-front image is concerned. The correction for time, t, is the accumulated increase in distance on the film, $x_1 - x_0$, $x_2 - x_0$, $x_3 - x_0$, etc., divided by the slit velocity, U_f. For shock-front image motion in the opposite direction (lower row of frames), it is seen that the time between frames decreases for the shock-front image.

TABLE A-2. THE INSTANTANEOUS SHOCK VELOCITY, U_s, THE AVERAGE SHOCK VELOCITY, $\bar{U}_s$, AND MOTION CORRECTION, Δx, AS A FUNCTION OF x FOR TWO SLIT WIDTHS AND THREE SHOCK DIRECTIONS

		$U_s \downarrow$ $U_f \downarrow$				$U_s \uparrow$ $U_f \downarrow$				$-U_s$ $U_f \downarrow$	
		W = 1.02 mm		2.03 mm		1.02 mm		2.03 mm		2.03 mm	
x mm	U_s mm/μs	$\bar{U}_s$ mm/μs	Δx mm	$\bar{U}_s$ mm/μs	Δx mm	$\bar{U}_s$ mm/μs	Δx mm	$\bar{U}_s$ mm/μs	Δx mm	$\bar{U}$ mm/μs	Δx mm
0	6.053	5.756	2.84	5.543	5.41	5.802	2.34	5.611	4.52	5.547	4.90
2	5.618	5.385	2.63	5.210	5.06	5.419	2.20	5.263	4.26	5.215	4.60
4	5.254	5.067	2.46	4.922	4.75	5.094	2.08	4.964	4.04	4.928	4.35
6	4.945	4.793	2.32	4.671	4.49	4.825	1.98	4.705	3.84	4.677	4.13
8	4.679	4.554	2.19	4.451	4.26	4.570	1.88	4.479	3.67	4.457	3.94
10	4.448	4.344	2.09	4.256	4.06	4.357	1.80	4.279	3.52	4.262	3.76
15	3.987	3.917	1.86	3.857	3.65	3.925	1.63	3.871	3.21	3.861	3.41
20	3.641	3.592	1.70	3.548	3.34	3.598	1.50	3.558	2.96	3.552	3.14
25	3.374	3.338	1.57	3.305	3.10	3.341	1.40	3.312	2.77	3.308	2.92
30	3.160	3.133	1.47	3.108	2.90	3.136	1.32	3.112	2.61	3.110	2.75
35	2.987	2.966	1.39	2.946	2.74	2.968	1.25	2.950	2.48	2.948	2.60
40	2.843	2.827	1.32	2.810	2.61	2.828	1.20	2.813	2.37	2.812	2.48
50	2.620	2.609	1.21	2.598	2.40	2.610	1.11	2.600	2.20	2.599	2.29
60	2.455	2.447	1.13	2.439	2.25	2.447	1.04	2.440	2.07	2.440	2.15
70	2.328	2.322	1.07	2.316	2.13	2.322	0.99	2.317	1.97	2.317	2.05
80	2.228	2.224	1.03	2.219	2.04	2.224	0.95	2.220	1.89	2.219	1.96
90	2.147	2.144	0.99	2.140	1.96	2.144	0.92	2.140	1.82	2.140	1.89
100	2.081	2.078	0.96	2.075	1.90	2.078	0.89	2.076	1.77	2.075	1.85
110	2.025	2.021	0.93	2.020	1.85	2.023	0.87	2.021	1.73	2.021	1.78
120	1.978	1.977	0.91	1.974	1.80	1.977	0.85	1.975	1.69	1.975	1.74

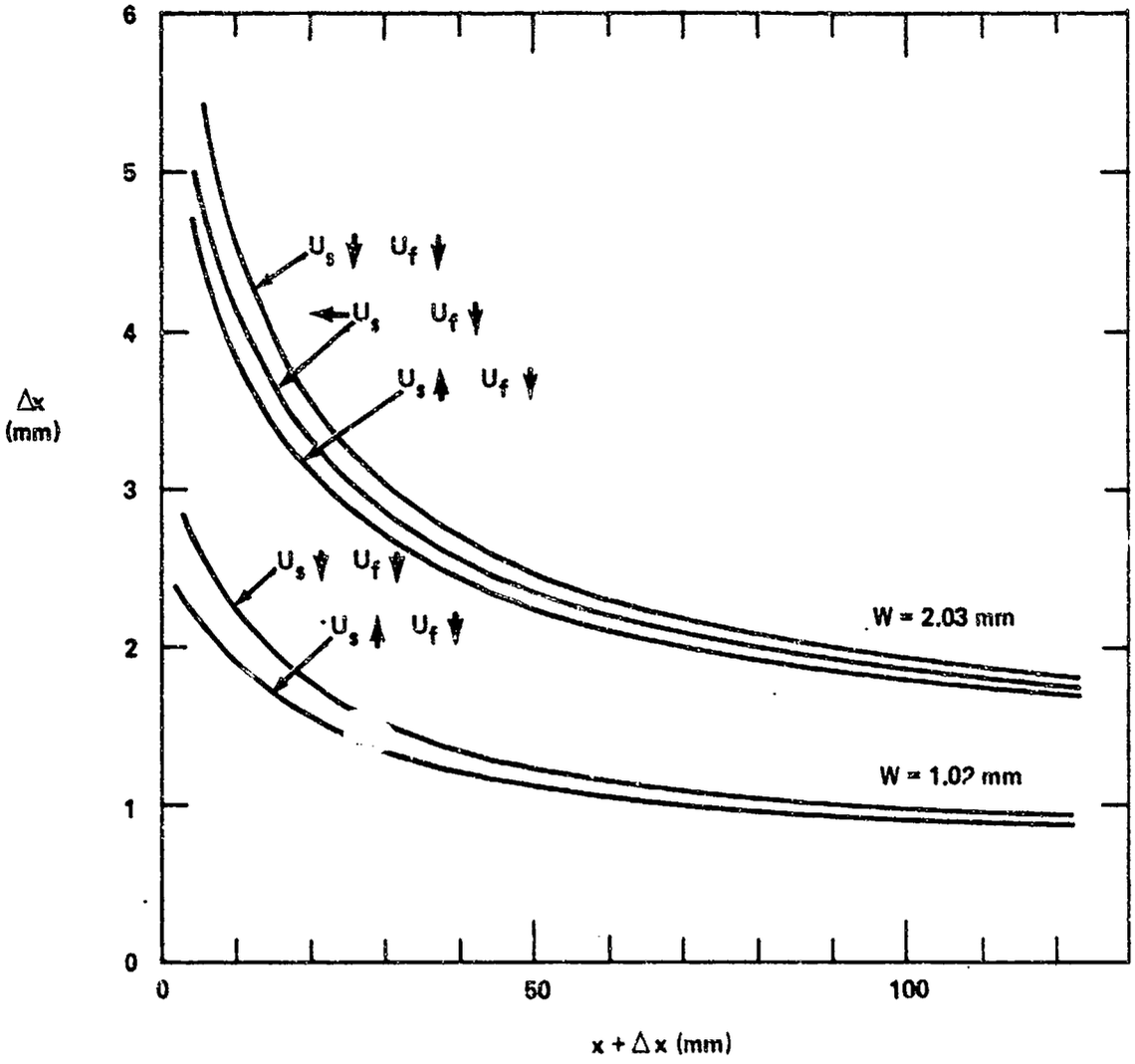

FIGURE A-3. POSITION CORRECTION CURVES, Δx VS $x + \Delta x$, FOR TWO SLIT WIDTHS AND THREE DIRECTIONS OF SLIT MOTION

TABLE A-3. CORRECTED x-t DATA FROM EIGHT EXPERIMENTS HAVING FOURTEEN USABLE SEQUENCES (x in mm, t in μs)

SEQUENCE 1		2		3		4		5		6		7	
x	t	x	t	x	t	x	t	x	t	x	t	x	t
10.5	3.81	17.3	7.56	12.2	3.84	4.0	3.56	9.2	3.47	14.1	7.02	11.1	3.63
24.3	7.68	30.3	11.41	26.2	7.72	18.3	6.95	22.5	6.88	27.6	10.41	25.1	7.26
36.6	11.51	42.1	15.24	38.6	11.56	30.5	10.36	33.4	10.32	38.1	13.86	36.1	10.88
47.6	15.33	52.6	19.32	48.8	15.36	40.5	13.82	43.5	13.77	47.5	17.33	46.3	14.51
56.9	19.13	61.4	22.83	58.6	19.17	49.6	17.30	52.8	17.25	56.4	20.81	55.6	18.14
66.5	22.92	70.5	26.61	68.0	22.96	58.8	20.77	61.4	20.77	64.7	24.29	64.6	21.77
75.7	26.70	78.7	30.28	77.2	26.74	67.3	24.25	69.4	24.21	72.9	27.78	73.1	25.39
83.5	30.47	87.2	34.16	85.4	30.51	75.0	27.75	77.3	27.71	80.7	31.28	80.8	29.02
92.0	34.24	95.1	37.92	93.3	34.28	83.1	31.24	84.9	31.21	88.5	34.78	88.8	32.65
99.9	38.01	102.9	41.69	101.2	38.05	90.8	34.74	92.6	34.74	95.6	38.29	97.0	36.28
107.2	41.77	110.5	45.46	108.9	41.85	97.8	38.29	100.0	38.22	102.9	41.78	104.2	39.91
114.8	45.52	118.1	49.21	116.7	45.57	105.2	41.74	107.0	41.72	110.1	45.29	111.3	43.53
122.6	49.28	-	-	124.1	49.33	112.2	45.25	113.9	45.24	117.0	48.80	-	-
-	-	-	-	-	-	119.3	48.76	120.9	48.74	123.7	52.32	-	-
-	-	-	-	-	-	126.5	52.27	-	-	-	-	-	-

SEQUENCE 8		9		10		11		12		13		14	
x	t	x	t	x	t	x	t	x	t	x	t	x	t
12.5	3.42	1.3	3.61	5.4	3.72	10.1	3.81	5.9	3.52	7.6	3.58	11.7	3.43
25.6	6.83	16.9	6.97	21.2	7.62	25.2	7.69	19.4	6.90	20.5	6.96	24.4	6.84
36.9	10.26	29.4	10.38	34.4	11.46	37.9	11.52	31.3	10.31	31.7	10.38	35.3	10.27
47.0	13.72	40.1	13.83	45.3	15.28	49.0	15.34	41.4	13.75	41.9	13.82	44.6	13.74
55.5	17.20	49.5	17.57	55.2	19.34	58.9	19.41	50.7	17.49	50.5	17.56	54.0	17.20
63.8	20.69	58.1	20.78	64.8	22.87	67.2	22.91	59.6	20.68	59.3	20.77	61.8	20.70
71.8	24.18	66.4	24.26	73.1	26.63	76.6	26.69	68.2	24.14	67.5	24.24	70.0	24.17
79.5	27.67	74.4	27.76	81.6	30.40	85.2	30.46	76.3	27.62	-	-	78.0	27.66
87.4	31.17	82.3	31.25	90.4	34.18	93.0	34.22	84.0	31.11	-	-	85.8	31.16
94.8	34.68	90.1	34.75	98.1	37.94	100.9	37.99	-	-	-	-	-	-
102.3	38.18	97.3	38.26	105.6	41.69	-	-	-	-	-	-	-	-
-	-	104.2	41.76	-	-	-	-	-	-	-	-	-	-

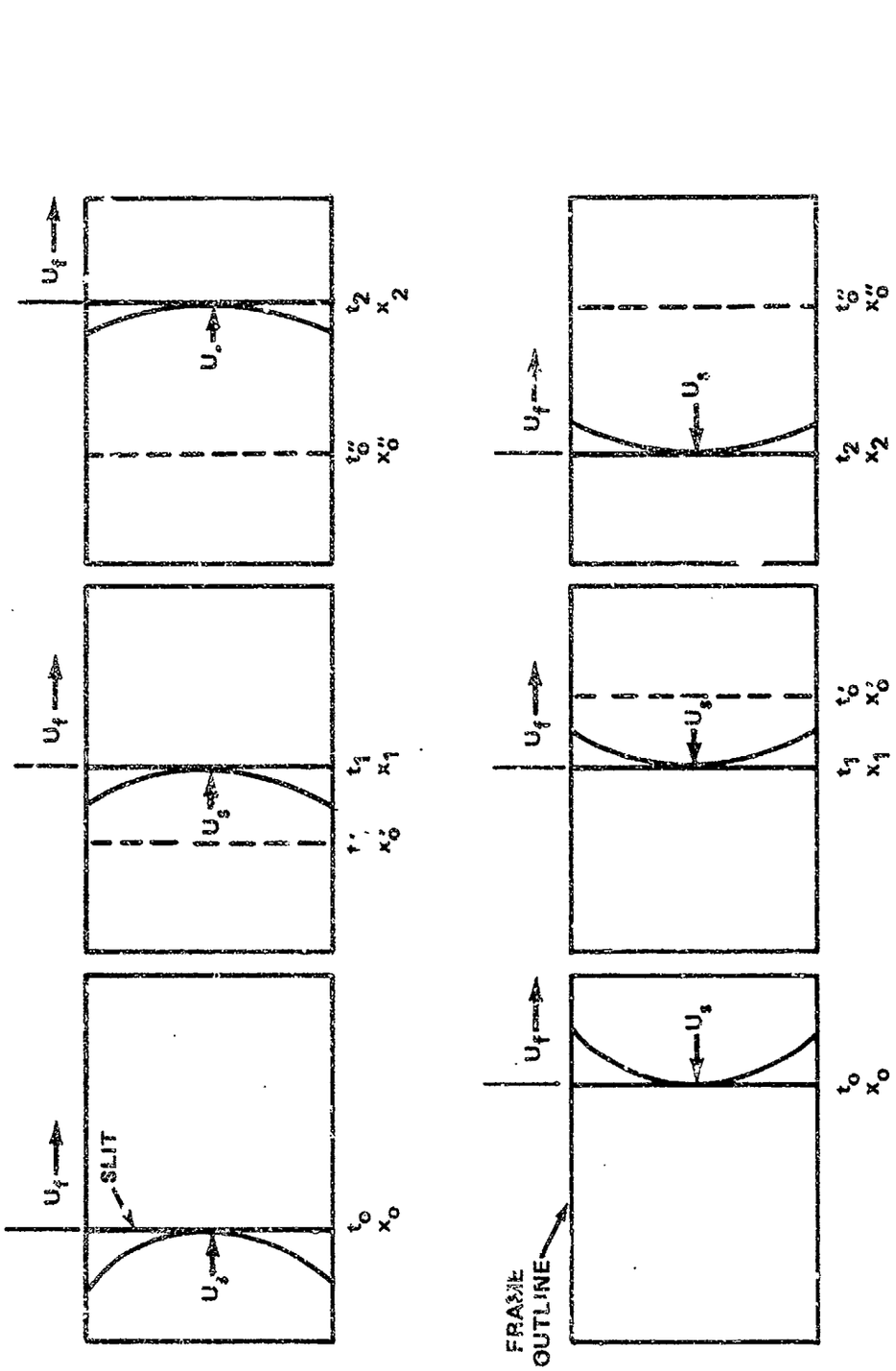

FIGURE A-4. INTERFRAME-TIME ERRORS CAUSED BY SHOCK-FRONT MOTION IN THE DIRECTION OF SLIT MOTION AND IN THE OPPOSITE DIRECTION

In the preceding paragraph it is assumed that the spacing between the position of x_0 on adjacent frames is always the same. In reality this is not so since minor variations in frame spacing are inherent in the camera. In the analysis in this report these variations make no significant difference in fitting a curve to the x-t data. Therefore, this correction is ignored in our analysis. However, the variation in frame spacing can lead to relatively large time errors in some applications, especially when only a few frames are available in a sequence.

APPENDIX B

THE SELECTION OF SEVERAL ANALYTICAL FORMS FOR FITTING SHOCK VELOCITY-TO-DISTANCE DATA

If U_S, from Table 2, is plotted as a function of 1/x, Figure B-1, it is seen that a nearly straight line can be drawn through most of the datum points between x = 40 and 120 mm. The equation for this line is

$$U_S = c' \left(1 + \frac{A'}{x}\right) \tag{B-1}$$

where

c' A' = the slope and
c' = the U_S-axis intercept.

The values of c' and A' are determined by a least squares fit to the data in Table 2. In the range of x = 50 to 100 mm, the value of c' is 1.5762 mm/μs and A' is 32.493 mm with a quadratic mean error (QME) of 0.0025. This is an extremely good fit. From x = 40 to 120 mm, c' is 1.5739 and A' is 32.306 with a QME of 0.0153; a good fit. However, for x less than 40 mm the fit is not good. This is expected, of course, since as x approaches zero, the calculated velocity approaches infinity. The calculated velocities, using Equation (B-1), are compared with the measured velocities in Table B-1. The velocities listed correspond to data in the range of x = 50 to 100 mm used to calculate c' and A'.

Although Equation (B-1) is not valid for x much less than 40 mm, it can be used as a means of checking all of the x-t data sets for consistency and for adjusting all of the x-t data so that they can be compared in a single x-t plot. Equation (B-1) is the only expression out of the several considered in which x can be calculated with reasonable ease. To obtain x, the Equation is first put in the differential form, $xdx/(x + A') = c'dt$. On integrating,

$$K = c't + A'\ln(x + A') - x. \tag{B-2}$$

Since there is no direct algebraic solution for x, Newton's Method of solution to f(x) = 0 is used, i.e.,

$$f(x) = x - A'\ln(x + A') + K - c't = 0. \tag{B-3}$$

One can solve for the constant of integration, K, in Equation (B-2) by using previously determined values of c' and A' and the corrected values of x and t from Table A-3, Appendix A. It is found that K is fairly constant for values of x ranging from 30 to 125 mm. The mean value of K, i.e., $\bar{K}$, is determined over this constant-value range for each x-t set. However, the value of $\bar{K}$ is observed to vary considerably from set to set. This occurs because the values of t are taken

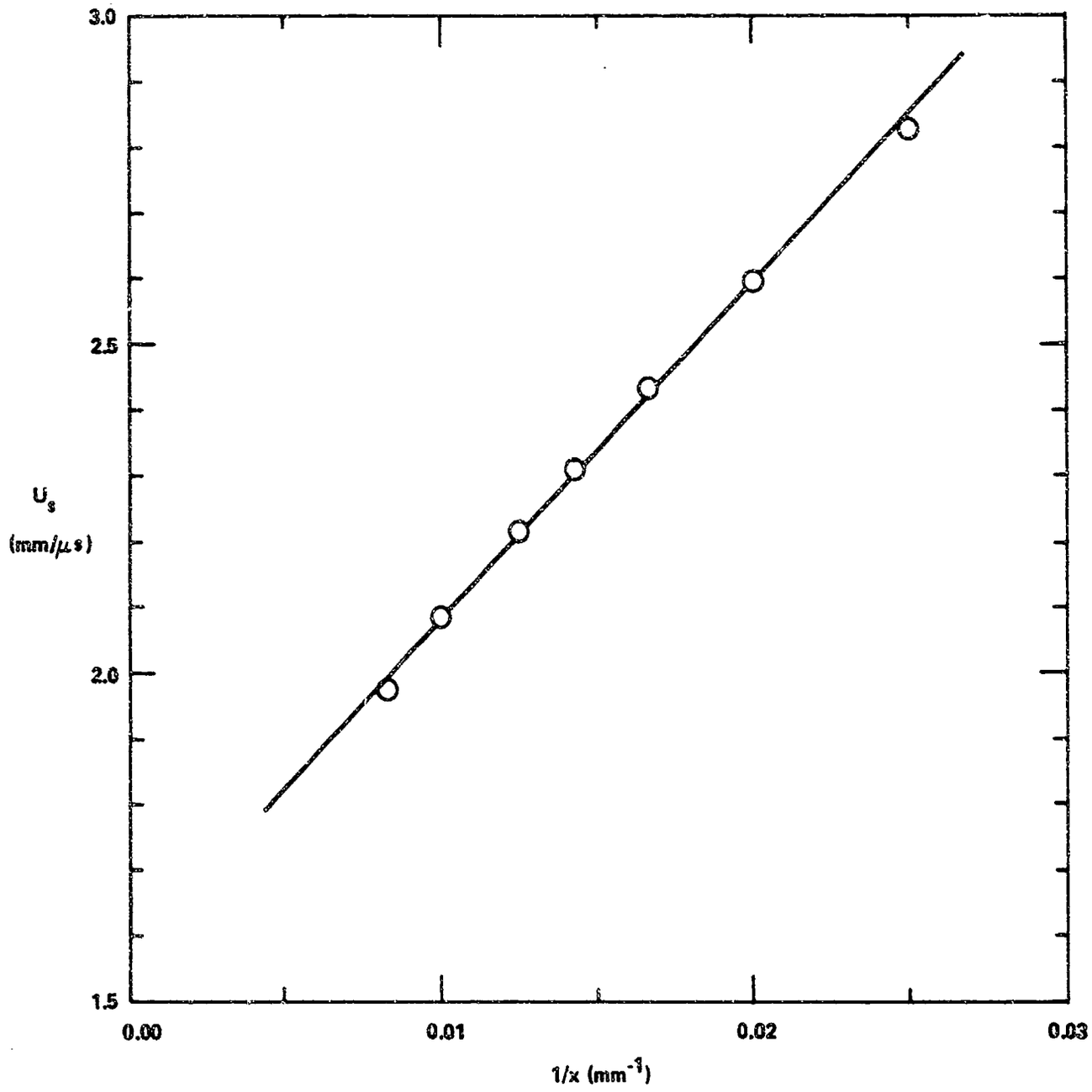

FIGURE B-1. THE SHOCK VELOCITY, U_s, AS A FUNCTION OF 1/x FROM EQUATION (B-1) AND THE MEASURED VELOCITIES

TABLE B-1. COMPARISON OF MEASURED AND CALCULATED VALUES OF U_s USING EQUATIONS (B-1) AND (B-4)

x (mm)	SHOCK VELOCITY, U_s (mm/μs) MEAS.	EQ. (B-1)	EQ. (B-4)
10	4.405	6.698	4.405
20	3.649	4.137	3.642
30	3.157	3.283	3.159
40	2.829	2.857	2.836
50	2.596	2.601	2.608
60	2.434	2.430	2.440
70	2.311	2.308	2.313
80	2.218	2.216	2.213
100	2.084	2.088	2.067
120	1.975	2.003	1.967

to be evenly spaced interframe times, before corrections are made, and x = 0, t = 0 can fall anywhere between the frames. Actually, the time at which shock-front motion begins can not be pin-pointed on any one record. At the start the shock velocity is about 6 mm/μs, but it decays rapidly. Thus, in the first 10 mm of travel, the shock-front image is recorded in only one frame, or none at all. In fact, out of the fourteen sequences, there are only six shock-front images recorded within the first 10 mm of travel.

All of the x-t data can be put in proper time correspondence by subtracting the value of t found at x = 0 in Equation (B-2) from the values of t listed for each x-t set in Table A-3, Appendix A. When the adjustments are made, the value of $\bar{K}$ is found to equal 113.1089 mm for all of the x-t sets. The adjusted x-t data are plotted in Figure B-2. The close-in shape of the x-t curve is now apparent and the actual origin of the x-t curve is seen to be located at about t = -1.8 μs.

Finally, the corrected values of t from Table A-3 and the determined values of c' and A' are used in Equation (B-3) to calculate x. The results, x_{calc}, are compared with x_{exp}, i.e., $x_{exp} - x_{calc}$. The mean of the absolute value of $x_{exp} - x_{calc}$ is included in Table B-2 for the fourteen sequences. Also listed in Table B-2 are the amounts of time subtracted from t in Table A-3 to obtain the time adjustment used in the plot of Figure B-2.

It is useful to have an equation that fits the shock-wave versus x data over the range of 30-150 mm used in Underwater Sensitivity Tests. A form that does this up to at least 120 mm is

$$U_s = c_o \left(1 + \frac{A}{R_o + x^B} \right), \qquad \text{(B-4)}$$

where

R_o = 41.1 mm

A = 111.64322

B = 1.19226

The values of A and B are obtained from a least-squares fitting routine, over the range of x = 10 to 120 mm, which gives a QME of 0.0082 for the overall fit. This QME indicates that the fit is very good. A comparison of measured velocities and predicted velocities from Equation (B-4) is made in Table B-1. Note that Equation (B-4), the shock wave jump equations, and the equation of state of water are used, as previously described, to give a relation of peak shock pressure in water as a distance from the pentolite sphere.

It would be useful to hydrodynamics and underwater damage modelers to have a form for pressure versus scalable distance, R/R_o. This form would allow easy predictions of shock propagation in water for various size spheres of pentolite. To this end a few forms of shock velocity versus R/R_o are evaluated. Some additional shock-velocity data from pentolite spheres of 1.27 cm radius are included to allow the least-squares fitting of these forms over a range of R/R_o of 1.24 to 12.27. The following equations are evaluated.

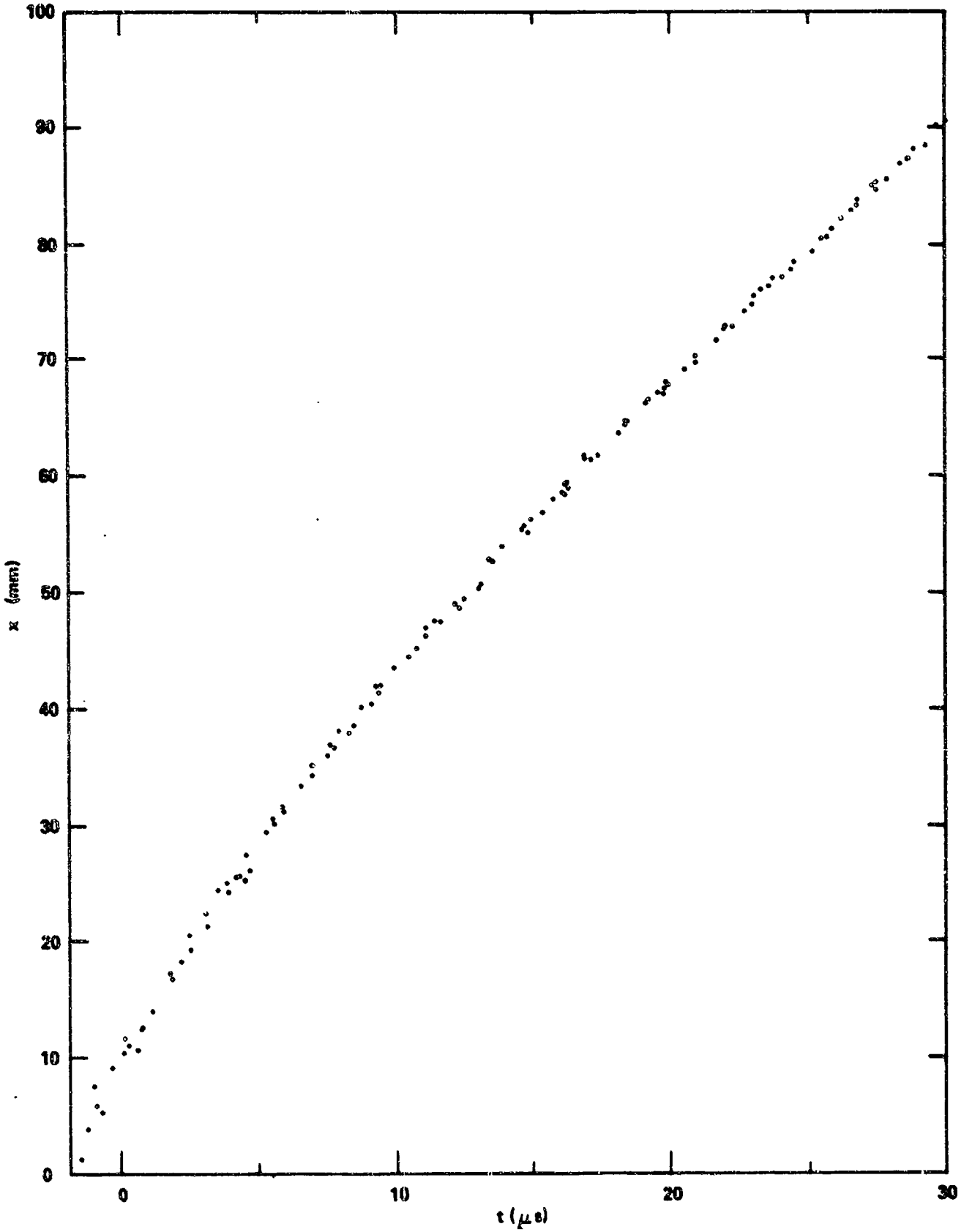

FIGURE B-2. THE MEASURED DISTANCE, X, AS A FUNCTION OF t ADJUSTED TO X=0 IN EQUATION (B-2)

TABLE B-2. THE AVERAGE DEVIATION OF $\bar{K}$, MEAN RESIDUAL OF x, AND THE TIME ADJUSTMENT FOR x = 0 FOR FOURTEEN SEQUENCES

SEQUENCE NO.	AV DEV OF $\bar{K}$ [a]	NO. OF ENTRIES	$\overline{\lvert x_{exp}-x_{calc} \rvert}$	t AT $x_i = 0$ (μs) [b]
1	0.1588	11	0.23	-3.7175
2	0.1004	11	0.14	-5.7704
3	0.1833	11	0.27	-3.0573
4	0.1229	13	0.19	-4.7747
5	0.1553	12	0.23	-3.7861
6	0.1769	12	0.26	-5.8653
7	0.1129	10	0.16	-3.4071
8	0.1325	10	0.22	-2.5869
9	0.1184	10	0.19	-5.0821
10	0.1687	9	0.24	-4.4923
11	0.2376	8	0.36	-3.1908
12	0.2372	7	0.37	-4.3255
13	0.2700	5	0.47	-4.5228
14	0.2146	7	0.35	-3.2966

[a] $\bar{K}$ = 113.1089 mm, c' = 1.5762 mm/μs

[b] From Equation B-2

$$U_s = c_o \left[1 + \frac{A}{(R_1)^B} \right] \tag{B-5}$$

$$U_s = c_o \left[1 + \frac{K'(A + 1)}{A + R_1^B} \right] \tag{B-6}$$

$$U_s = c_o \left[1 + \frac{K'(A + 1)^B}{(A + R_1)^B} \right] \tag{B-7}$$

where $R_1 = R/R_o$.

Table B-3 gives the results of least-squares fitting these forms. The QME for Equation (B-5) is seen to be large which indicates that this form is not adequate over the entire range of R/R_o, i.e., 0 to ∞. However, it does fit the data very well over the range used in the Underwater Sensitivity Test. Equation (B-5) is implicitly used in the expression for P(R) in reference B-1. Although

TABLE B-3.

THE PARAMETERS, A, B, AND K', FOR EQUATIONS (B-5), (B-6), AND (B-7)

EQUATION	A	B	K'	QME
(B-5)	2.76523	1.60598	1.000000	0.02934
(B-6)	-0.354235	1.34374	4.474863	0.01294
(B-7)	-0.360619	1.28486	4.435364	0.01192

it does not fit the data quite as well as Equation (B-4), it was selected because, being scalable, it has a much wider application. (Note: If one derives A and B from the expression for P(R) found in reference B-1, the values will be somewhat different from those shown in Table B-3. These differences occur because the fit is over a shorter R/R_o range in the reference. In addition, more recent data and a more refined analysis technique are used in this report which adds slightly to the differences.)

B-1 Frankel, M. J., Liddiard, T. P., and Forbes, J. W., "Low-Level Reaction Thresholds in High Explosives and Propellants," Combustion and Flame, Vol. 45, No. 1, Jan 1982, p. 35.

As to the more recently derived expressions, the QME of the fits for Equation (B-6) and (B-7) are very good and about the same magnitude over the entire range from $R/R_0 = 1$ to ∞. This indicates that either form could be used to reproduce accurately the velocity over the entire range. All of the above equations involving U_s are forced to give the sound velocity in water (1.483 mm/μs at 20°C) for very large values of R_1. Equations (B-6) and (B-7) give shock velocities of 5.958 and 5.917 mm/μs, respectively, for $R_1 = 1$. These extrapolated values are very near the measured value of 6.053 mm/μs.

It also would be useful if the shock velocity at $R_1 = 1$ is set equal to the measured value of 6.053 mm/μs. This is easily done with Equations (B-6) and (B-7) by fixing K' at 3.0816 mm/μs and least-squares fitting for A and B. The results of this fitting are given in Table B-4. Note that the QME's of these two parameter fits are slightly higher than for the three parameter fits given in Table B-3.

TABLE B-4.

THE PARAMETERS, A AND B, FOR EQUATIONS (B-6) AND (B-7) WITH K' = 3.0816

EQUATION	A	B	QME
(B-6)	-0.406213	1.30135	0.01402
(B-7)	-0.434278	1.2231	0.01435

However, these QME's and consequential fits to the data are still quite good. To obtain a better appreciation of these fits, Table B-5 gives the measured data and the various calculated values. The two parameter fit for Equation (B-6) is chosen as the best overall representation of the data. This equation combined with Equation (2) in the text gives the peak shock pressure as a function of R/R_0.

TABLE B-5. A COMPARISON OF FITS OF SEVERAL OF THE EQUATIONS CONSIDERED

	SHOCK VELOCITY, U_s (mm/μs)					
R/R_o	MEAS.	EQ.(B-5)	EQ.(B-6)[a]	EQ.(B-7)[a]	EQ.(B-6)[b]	EQ.(B-7)[b]
1.243	4.405	4.375	4.416	4.415	4.429	4.435
1.487	3.649	3.651	3.623	3.626	3.620	3.621
1.730	3.157	3.183	3.149	3.150	3.143	3.141
1.973	2.829	2.860	2.835	2.834	2.830	2.827
2.217	2.596	2.625	2.612	2.611	2.608	2.606
2.460	2.434	2.449	2.447	2.446	2.445	2.443
2.703	2.311	2.313	2.321	2.319	2.320	2.319
2.946	2.218	2.206	2.221	2.220	2.222	2.221
3.433	2.084	2.049	2.074	2.073	2.076	2.077
3.920	1.975	1.940	1.972	1.972	1.975	1.977
8.015	1.686	1.628	1.663	1.666	1.669	1.674
12.269	1.583	1.556	1.584	1.587	1.589	1.594

[a] LSQ fitted parameters from Table B-3

[b] LSQ fitted parameters from Table B-4

APPENDIX C

WEAK-SHOCK SOLUTION FOR EXPLOSIVELY GENERATED SHOCK WAVES IN WATER

In the work of Rogers[C-1] it is shown that the peak pressure of a weak shock wave is given by the expression

$$P = P_1 \frac{\{[1 + 2(R_1/\ell_o)\ \ln(R/R_1)]^{\frac{1}{2}} - 1\}}{(R/\ell_o)\ \ln(R/R_1)}, \qquad \text{(C-1)}$$

where

P_1 = the peak pressure of the shock at distance, R_1, from center of charge

ℓ_o = the characteristic length = $\rho_o\ c_o^3\ \tau_1/P_1\beta$

ρ_o = the initial density

c_o = the sound velocity

β = the parameter of non-linearity of a fluid.

The expression for the pulse time constant is

$$\tau = \tau_1\ [1 + 2(R_1/\ell_o)\ \ln(R/R_1)]^{\frac{1}{2}} \qquad \text{(C-2)}$$

It is not obvious that these two equations scale for explosive charges of different initial sizes. However, the gage data of Table 4 in the text show that P_1 and τ/R_o are approximately constant at the scaled distance, R_1/R_o. For a reference shock pulse (P_1, R_1, τ_1), R_1/R_o also is a constant. Then, $\ell_o = \tau_1 K_o = R_o K_1 = R_1 K_2$, where $K_o = \rho c_o^3/P_1$, K_1 and K_2 are unknown constants for a given reference state (P_1, R_1, τ_1). Substituting these simplifications into Equation (C-1) results in

$$\frac{P}{P_1} = \frac{\{[1 + 2K_3\ \ln(R/R_1)]^{\frac{1}{2}} - 1\}}{(R/R_1)K_3\ \ln(R/R_1)} \qquad \text{(C-3)}$$

C-1 Rogers, P. H., "Weak-Shock Solution for Underwater Explosive Shock Waves," Journal of the Acoustical Society of America, Vol. 62, 1977, pp. 1412-1419.

$$\tau = \tau_1 [1 + 2K_3 \ln(R/R_1)]^{\frac{1}{2}} \qquad \text{(C-4)}$$

where $K_3 = 1/K_2$, an unknown factor. Equations (C-3) and (C-4) are preferable when fitting to weak-shock data. Note that these equations were derived using weak-shock approximations and the assumption that the pulse shape is exponentially decaying in time. These assumptions limit the general usefulness of the equations, but, the work of Rogers is a large step forward in treating weak shocks in water.

Tables C-1 and C-2 give the results of fitting the shock-velocity data of Table 2 in the text to Equation (C-3) for two different reference shock pulses. It is clear that Equation (C-3) gives a fair fit to the peak pressure data for P_1 = 19.1 and 14.1 kbar. Equation (C-3) fits the data better for the lower reference shock with peak pressure of 14.1 kbar. It is expected that Equation (C-3) will closely reproduce the peak pressure data for pressures less than a few kilobars.

Equation (C-3) also was fitted to the lower pressure gage data of Table 4 in the text. The results of a least-squares fit of Equation (C-3) to the data is given in Table C-3. As expected, this fit is better than that indicated by the results given in Table C-1 or Table C-2, since it was made over a lower pressure range.

The decay time (pulse half-width), τ, given in Table 4, is the time taken for the pressure to fall one-half of its peak value. Equation (C-4) can be used to calculate this τ if the shock decay is exponential and τ_0 is chosen as the pulse width at half the peak pressure. Note that the constant, K_3 = 1.9, was obtained by fitting the pressure data. The calculated values of τ/R_0 are given in Table C-3, along with the measured τ/R_0 data from Table 4. These values are within 10 to 20% of the measured values. An improvement in reproducing the data, using Equation (C-4), would be expected if more realistic shock profiles were used in the derivation of Equation (C-4).

TABLE C-1. WEAK SHOCK-WAVE PEAK PRESSURE FOR $P_1 = 19.1$, $R/R_o = 1.973$, AND $K_3 = 4.7$

$\frac{R}{R_o}$	P (kbar)*	P_{calc} (kbar)	$P-P_{calc}$ (kbar)
2.217	14.3	13.89	0.41
2.460	11.4	11.13	0.27
2.703	9.4	9.33	0.07
2.946	8.0	8.04	-0.04
3.433	6.1	6.29	-0.19
3.920	4.7	5.15	-0.45
8.02	1.63	1.97	-0.34
12.27	0.75	1.17	-0.42

*Obtained from Table 2 in text.

TABLE C-2. WEAK SHOCK-WAVE PEAK PRESSURE FOR $P_1 = 11.4$, $R_1/R_o = 2.46$, AND $K_3 = 2.9$

$\frac{R}{R_o}$	P (kbar)*	P_{calc} (kbar)	$P-P_{calc}$ (kbar)
2.703	9.4	9.25	0.15
2.946	8.0	7.83	0.17
3.433	6.1	6.02	0.08
3.920	4.7	4.89	-0.19
8.02	1.63	1.84	-0.21
12.27	0.75	1.09	-0.34

*Obtained from Table 2

TABLE C-3. MEASURED SHOCK-WAVE PROFILES IN WATER FROM THREE SIZES OF PENTOLITE SPHERES

$\frac{R}{R_o}$	R_o (cm)	MEAS. PK. PRESSURE (kbar)	CALC. PK. PRESSURE (kbar)*	MEAS. τ/R_o (μs/cm)	CALC. τ/R_o (μs/cm)
4.97	4.11	3.048	3.052	6.00	7.25
6.50	6.84	2.038	2.003	8.36	9.44
8.01	4.11	1.543	1.490	11.73	10.84
8.01	6.84	1.449	1.490	9.63	10.84
8.02	1.27	1.447	1.487	9.83	10.85
12.27	1.27	0.803	0.851	12.01	13.25
12.28	4.11	0.817	0.850	12.18	13.25

*Reference state of P_1 = 3.823 kbar, R_1/R_o = 4.39, $1\tau/R_o$ = 5.98, and K_3 = 1.9

DISTRIBUTION

	Copies
Commander	
Naval Air Systems Command	
Attn: Library	1
AIR-350 (H. Benefiel)	1
AIR-5411A	1
Washington, D. C. 20361	
Commander	
Naval Sea Systems Command	
Attn: PMS-400M	1
SEA-403	1
SEA-04H	1
SEA-09G32	1
SEA-06R (D. J. Pastine)	1
SEA-63R (F. Ramano)	1
SEA-62R32 (G. Edwards)	1
SEA-62YB	1
SEA-62Y13C	1
SEA-62Z	1
SEA-62Z31E	1
SEA-64E (R. Beauregard)	1
SEA-99612	2
Department of the Navy	
Washington, D. C. 20362	
Chief of Naval Material	
Attn: PM-23 (J. Amlie)	1
MAT-071 (O. Remson)	1
MAT-0716 (A. Faulstich)	1
Washington, D. C. 20362	
Commander	
Naval Weapons Center	
Attn: Code 3835 (R. G. Sewell)	1
Code 3205 (L. Smith)	1
Code 3262 (G. Greene)	1
Code 3264 (T. Joyner)	1
Code 385 (A. Amster)	1
Code 3261 (M. Wagenhals)	1
Technical Library	1
China Lake, CA 93555	

	Copies
Commander	
David W. Taylor Naval Ship Research and Development Center	
Attn: R. Garrison	1
Bethesda, MD 20084	
Commanding Officer	
Naval Explosive Ordnance Disposal Facility	
Attn: DL (G. Stevenson)	1
Indian Head, MD 20640	
Commanding Officer	
Naval Weapons Station	
Attn: L. Rothstein	1
Yorktown, VA 23691	
Superintendent	
Naval Postgraduate School	
Attn: Library	1
Monterey, CA 93940	
Commander	
Naval Research Laboratory	
Attn: Technical Information	1
Washington, D. C. 20375	
Commander	
Naval Intelligence Support Center	
Attn: NISC-30	1
4301 Suitland Road	
Washington, D. C. 20390	
Director	
Army Material Systems Analysis Agency	
Attn: DRXSY-D	1
DRXSY-J (J. McCarthy)	1
Aberdeen Proving Ground, MD 21005	

DISTRIBUTION (Cont.)

	Copies
Commander U. S. Army Armament Research and Development Command Attn: DRDAR-LCE (R. Walker) DRDAR-LCE-D (N. Slagg) DRDAR-LCE-D (L. Avrami) Dover, NJ 07801	1 1 1
Air Force Armament Test Laboratory Attn: DLYV (A. Rutland) DLDE (L. Elkins) DLJW (R. McGuire) Eglin Air Force Base, FL 32542	1 1 1
Commanding Officer Ballistics Research Laboratory USARRADCOM Attn: Technical Library R. Frey P. Howe H. Reeves Aberdeen Proving Ground Aberdeen, MD 21005	1 1 1 1
Director Defense Advanced Research Projects Agency Attn: Library 1400 Wilson Boulevard Arlington, VA 22209	1
Chief of Naval Research Attn: ONR-432 (R. Miller) ONR-260 (D. Siegel) 800 North Quincy Street Arlington, VA 22217	1 1
Defense Technical Information Center Alexandria, VA 22314	12
Director Ballistics Research Laboratory Attn: DR/DAR (F. Grace) Aberdeen Proving Ground Aberdeen, MD 21005	1
Commander Naval Research Laboratory Attn: P. H. Rogers Orlando, FL 32806	1
Honeywell, Inc. Defense Systems Division Attn: J. Blackburn P. DiBona J. Doyle K. Doeringsfeld 600 Second Street, N. E. Hopkins, MN 55343	1 1 1 1
Washington State University Department of Physics Attn: R. Fowles Pullman, WA 99164	1
Sandia National Laboratories Attn: J. Asay J. Kennedy R. Graham Albuquerque, NM 87115	1 1 1
Los Alamos National Laboratory Attn: J. Shaner R. Rabie J. Johnson S. Goldstein W. C. Davis Los Alamos, NM 87545	1 1 1 1 1
University of California Lawrence Livermore National Laboratory Attn: E. L. Lee F. E. Walker R. J. Wasley P. O. Box 808 Livermore, CA 94550	1 1 1
Library of Congress Attn: Gift and Exchange Division Washington, D. C. 20540	4

DISTRIBUTION (Cont.)

		Copies
Internal Distribution:		
R13:	R. Bardo	1
	R. Bernecker	1
	A. R. Clairmont	1
	C. S. Coffey	1
	N. L. Coleburn	1
	D. Demske	1
	C. Dickinson	1
	W. Elban	1
	J. W. Forbes	10
	H. Jones	1
	K. Kim	1
	E. R. Lemar	1
	T. P. Liddiard	10
	P. J. Miller	1
	C. Richmond	1
	H. Sandusky	1
	D. Tasker	1
	J. W. Watt	1
	F. Zerilli	1
	D. Price	1
	S. Jacobs	1
R13		1
R11		1
R12		1
R14		1
R15		1
R16		1
R121		1
R122		1
R12:	J. Short	1
	J. Erkman	1
	L. Montesi	1
	E. Kilmer	1
	M. Lutzsky	1
	H. Sternberg	1
R14:	J. Gaspin	1
	D. O'Keeffe	1
	D. Lehto	1
R15:	R. Price	1
	R. Tussing	1
	G. Hammond	1
R44:	H. Glaz	1
	A. VanTuyl	1
U13:	J. Honaker	1
F34:	J. Sazama	1
G35		1
G35:	W. Holt	1
	W. Mock	1
G04:	W. Soper	1
G41:	W. A. Walker	1
E35 (GIDEP Office)		1
E431		9
E432		3